INTERNATIONAL ATOMIC ENERGY AGENCY
UNITED NATIONS EDUCATIONAL, SCIENTIFIC AND CULTURAL ORGANIZATION

INTERNATIONAL CENTRE FOR THEORETICAL PHYSICS
34100 TRIESTE (ITALY) - P.O.B. 586 - MIRAMARE - STRADA COSTIERA 11 - TELEPHONES: 224281/2/3/4/5/6
CABLE: CENTRATOM - TELEX 460392-I

SMR/115 - 48

WINTER COLLEGE ON LASERS, ATOMIC AND MOLECULAR PHYSICS

(21 January - 22 March 1985)

HIGH-RESOLUTION SUB-DOPPLER LASER SPECTROSCOPY

W. DEMTROEDER
Fachbereich Physik
Universitaet Kaiserslautern
Postfach 3049
6750 Kaiserslautern
Fed. Rep. Germany

These are preliminary lecture notes, intended only for distribution to participants.
Missing or extra copies are available from Room 229.

10. High-Resolution Sub-Doppler Laser Spectroscopy

The spectral resolution of all methods discussed in Chap.8 was in principle limited by the Doppler width of lines in the molecular absorption—or emission—spectra, although the laser linewidth might have been much smaller. In this chapter we present several techniques which overcome this resolution limit and which allow one to resolve the natural linewidth even in the presence of a much larger Doppler width. These techniques, which have been developed recently, have already stimulated experimental and theoretical atomic physics in an outstanding way. These various Doppler-free methods certainly represent an important step towards a more detailed knowledge of molecular structure and of deeper details regarding the interaction of E.M. radiation and matter.

While for most experiments in Doppler-limited spectroscopy—discussed in Chaps.8 and 9—*multimode* lasers can be used (e.g., for optical pumping experiments, laser-induced fluorescence of atoms and simple molecules, or for Doppler-limited absorption spectroscopy) only some of the sub-Doppler methods, treated in this chapter, may be performed with pulsed or cw multimode lasers. Most of these techniques demand narrow-band tunable *single-mode* lasers with a bandwidth which should be smaller than the desired spectral resolution. If the natural linewidth $\delta\nu_n$ has to be resolved, the laser frequency jitter should be smaller than $\delta\nu_n$. This demands frequency stabilization techniques (see Sect.6.5) and there are many examples in this branch of high-resolution laser spectroscopy where the achieved resolution is indeed limited by the stability of the laser.

The basic principle of most Doppler-free techniques relies on a proper selection of a subgroup of molecules with velocity components v_z in the direction of the incident monochromatic wave, which fall into a small interval Δv_z around $v_z = 0$. This selection can be achieved either by mechanical apertures which select a collimated molecular beam, or by selective saturation within the velocity distribution of absorbing molecules caused by a strong pump wave, and a successive probing of this selective "hole burning" by a monochromatic tunable probe wave (see Sect.3.6).

Another class of Doppler-free techniques is based on a coherent preparation of an atomic or molecular state and a detection scheme which is capable of detecting the phase relations of the wave functions in this state. Most of these "coherent excitation methods" rely on optical pumping by pulsed or cw lasers, which may not even be single-mode lasers as long as the selective population of the levels under study is guaranteed.

We will now discuss these different methods in more detail.

10.1 Spectroscopy in Collimated Molecular Beams

Let us assume molecules effusing into a vacuum tank from a small hole A in an oven which is filled with a gas or vapor at pressure p. The molecular density behind A and the background pressure in the vacuum tank shall be sufficiently low to assure a large mean free path of the effusing molecules, such that collisions can be neglected. The number $N(\vartheta)$ of molecules which travel into the cone $\vartheta \pm d\vartheta$ around the direction ϑ against the symmetry axis (which we choose to be the z axis) is proportional to $\cos\vartheta$. A slit B with width b selects at a distance d from the point source A a small angular interval $-\varepsilon \leq \vartheta \leq +\varepsilon$ around $\vartheta = 0$ (see Fig.10.1). The molecules passing through the slit B, which is parallel to the y axis, form a molecular beam in the z direction, collimated with respect to the x direction. The collimation ratio is defined by (see Fig.10.1b)

$$v_x/v_z = \tan\varepsilon = b/(2d) \quad . \tag{10.1}$$

If the source diameter is small compared with the slit width b and if $b \ll d$ (which means $\varepsilon \ll 1$), the flux density behind the slit B is approximately constant across the beam diameter, since $\cos\vartheta \approx 1$ for $\vartheta \ll 1$. For this case the density profile of the molecular beam is illustrated in Fig.10.1b.

The density $n(v)dv$ of molecules with velocities $v = |\underline{v}|$ inside the interval v to v + dv in a molecular beam at thermal equilibrium which effuses with a most probable velocity $v_p = (2kT/m)^{1/2}$ into the z direction can be described at a distance $r = (z^2 + x^2)^{1/2}$ from the source A as

$$n(v,r)dv = C\,\frac{\cos\vartheta}{r^2}\,Nv^2\,e^{-(v/v_p)^2}\,dv \quad , \tag{10.2}$$

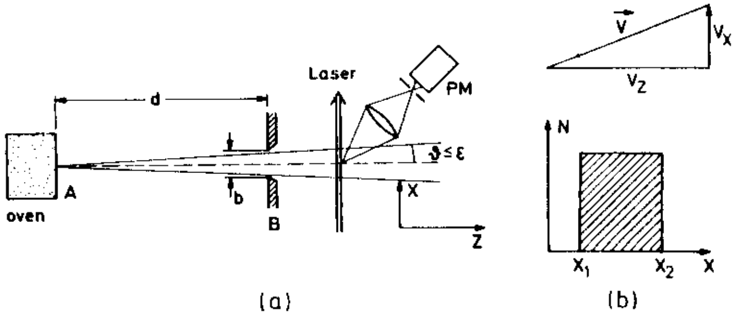

Fig.10.1. Schematic illustration of laser excitation spectroscopy with reduced Doppler width in a collimated molecular beam (a). Collimation ratio and density profile n(x) in a collimated beam effusing from a point source (b)

where the normalization factor $C = (4/\sqrt{\pi})v_p^{-3}$ assures that the total density N of the molecules is $N = \int n(v)dv$.

10.1.1 Reduction of Doppler Width

If the collimated molecular beam is crossed perpendicularly with a monochromatic laser beam with frequency ω propagating into the x direction, the absorption probability for each molecule depends on its velocity component v_x. In Sect.3.2 it was shown that the center frequency of a molecular transition, which is ω_0 in the rest frame of the moving molecule, is Doppler shifted to a frequency ω_0' according to

$$\omega_0' = \omega_0 - \underline{k}\underline{v} = \omega_0 - kv_x \quad ; \quad k = |\underline{k}| \quad . \tag{10.3}$$

Only those molecules with velocity components v_x in the interval $dv_x = \delta\omega_n/k$ around $v_x = (\omega - \omega_0)/k$ essentially contribute to the absorption of the monochromatic laser wave, because these molecules are shifted into resonance with the laser frequency ω within the natural linewidth $\delta\omega_n$ of the absorbing transition.

When the laser beam in the x-z plane passes along the x direction through the molecular beam at y = 0, its intensity decreases as

$$I(\omega) = I_0 \exp\left[-\int_{x_1}^{x_2} \alpha(\omega,x)dx\right] \quad . \tag{10.4}$$

For small absorptions the spectral profile of the absorbed intensity $dI = I(x_1) - I(x_2)$ is with $I(x_1) = I_0$

$$dI(\omega) = I_0 \int_{-v\sin\varepsilon}^{+v\sin\varepsilon} \left[\int_{x_1}^{x_2} n(v_x,x)\sigma(\omega,v_x)dx\right]dv_x \quad . \tag{10.5}$$

The absorption cross section $\sigma(\omega,v_x)$ describes the absorption of a monochromatic wave of frequency ω by a molecule with a velocity component v_x. Its spectral profile is represented by a Lorentzian (see Sect.3.6)

$$\sigma(\omega,v_x) = \sigma_0 \frac{(\gamma/2)^2}{(\omega - \omega_0 - kv_x)^2 + (\gamma/2)^2} = \sigma_0 \cdot L(\omega - \omega_0,\gamma) \quad . \tag{10.6}$$

The density $n(v_x,x)dv_x$ of molecules with velocity components v_x in the interval dv_x at a point (x,z) in the molecular beam can be derived from (10.2). Using the relations $r^2 = x^2 + z^2$; $v_x/v = x/r \rightarrow dv_x = (x/r)dv$ we obtain with $\cos\vartheta = z/r$ (note that dv_x changes sign with x since $dv > 0$)

$$n(v_x,x)dv_x = CN \frac{z}{x^3} v_x^2 \, e^{-(rv_x/xv_p)^2} \, dv_x \quad . \tag{10.7}$$

Equation (10.3) gives the relation between the velocity component v_x and the Doppler shift $\Delta\omega_0 = \omega_0 - \omega_0' = kv_x = v_x\omega_0/c$ of the center frequency ω_0.

Inserting (10.3,6,7) into (10.5) yields the absorption profile

$$dI(\omega) = a \int_{-\infty}^{+\infty} \left\{\int_{x_1}^{x_2} \frac{\Delta\omega_0^2}{x^3} L(\omega - \omega_0,\gamma) \exp\left[-\Delta\omega_0^2 c^2/\omega_0^2 v_p^2\left(1 + \frac{z^2}{x^2}\right)\right] dx\right\} d(\Delta\omega_0) \tag{10.8}$$

with $a = I_0 cN\sigma_0(c^3/\,{}^3_0)z$. The integration over $\Delta\omega_0$ extends from $-\infty$ to $+\infty$ since the velocities v in (10.5) range from 0 to ∞. The integration over x can be carried out and gives with $x_1 = r\sin\varepsilon$, $r^2 = x^2 + z^2$

$$dI(\omega) = I_0 b \int_{-\infty}^{+\infty} L(\omega - \omega_0,\gamma) \exp-\left[(\omega - \omega')c/\omega_0 vp\sin\varepsilon\right]^2 d\omega' \tag{10.9}$$

with

$$b = a(zc/\omega_0)^2 \quad .$$

This represents a *Voigt profile*, i.e., a convolution product of a Lorentzian function with halfwidth γ and a Doppler function. A comparison with (3.33) shows, however, *that the Doppler width is reduced by a factor* $\sin\varepsilon$, which equals the collimation ratio of the beam. The collimation of the molecular beam therefore reduces the Doppler width $\Delta\omega_0$ of the absorption lines to a width

$$\boxed{\Delta\omega_D^* = \Delta\omega_D \sin\varepsilon} \qquad \text{with} \qquad \Delta\omega_D = 2\omega_0(v_p/c)(\ln 2)^{1/2} \ , \qquad (10.10)$$

where $\Delta\omega_D$ is the corresponding Doppler width in a gas at thermal equilibrium. Note that for larger diameters of the oven hole A the density profile $n(x)$ of the molecular beam is no longer rectangular but decreases gradually beyond the limiting angles $\vartheta = \pm\varepsilon$. For $\Delta\omega_D^* > \gamma$ the absorption profile is altered compared to that in (10.9), while for $\Delta\omega_D^* \ll \gamma$ the difference is negligible because the Lorentzian profile is dominant in the latter case [10.1].

The technique of reducing the Doppler width by the collimation of molecular beams was used before the invention of lasers to produce light sources with narrow emission lines (10.2). Atoms in a collimated beam had been excited by electron impact. The fluorescence lines emitted by the excited atoms show a reduced Doppler width if observed in a direction perpendicular to the atomic beam. However, the intensity of these atomic beam light sources was very weak and only the application of intense monochromatic tunable lasers has allowed one to take full advantage of this method of Doppler-free spectroscopy.

Figure 10.2 shows a typical experimental arrangement for sub-Doppler spectroscopy in molecular beams. The photomultiplier PM 1 monitors the total fluorescence $I_{Fl}(\lambda_L)$ as a function of the laser wavelength λ_L (excitation spectrum, see Sect.8.2), whereas PM 2 records the dispersed fluorescence spectrum excited at a fixed laser wavelength, where the laser is stabilized onto a molecular absorption line. A Fabry-Perot can be inserted to increase the spectral resolution of the fluorescence spectrum. A thorium hollow cathode spectral lamp serves as the wavelength calibration standard.

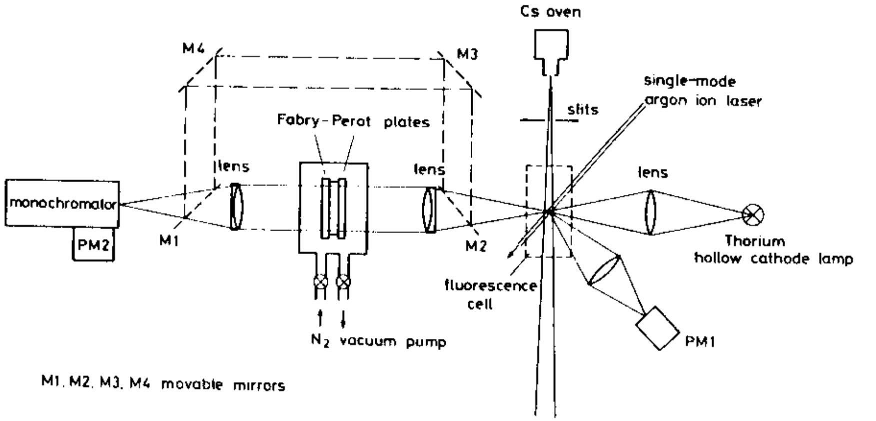

Fig.10.2. Typical experimental arrangement for sub-Doppler laser spectroscopy in collimated molecular beams

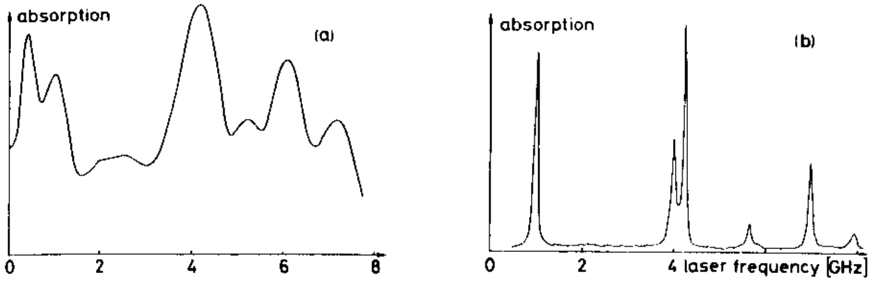

Fig.10.3a,b. Section of the excitation spectrum of the Cs_2 molecule in the spectral range around λ = 476.5 nm. (a) Excited in a cesium vapor cell, (b) excited in a collimated cesium beam

Figure 10.3 illustrates the achievable spectral resolution by comparing a section of the Cs_2 absorption spectrum obtained in a cesium vapor cell (left curve) and in a collimated cesium beam (right spectrum). Both spectra were taken with a single-mode argon laser which could be continuously tuned around λ = 476.5 nm. The absorption was monitored through the total fluorescence intensity $I_{Fl}(\lambda_L)$ as a function of laser wavelength λ_L (excitation spectroscopy, see Sect.8.2.1). The different lines correspond to rotational-vibrational transitions $(v'',J'') \rightarrow (v',J')$ between two different electronic states of the Cs_2 molecule [10.3].

Particularly for polyatomic molecules with their complex visible absorption spectra, the reduction of the Doppler width is essential for the resolution of single lines [10.4]. This is illustrated by a section from the excitation spectrum of the NO_2 molecule, excited with a single-mode tunable argon laser around λ = 488 nm (Fig.10.4). For comparison the same section of the spectrum as obtained with Doppler-limited laser spectroscopy in an NO_2 cell is shown in the upper trace [10.5].

Limiting the collimation angle of the molecular beam to 2×10^{-3} rad, the residual Doppler width can be reduced to 500 KHz. High-resolution iodine spectra with linewidths of less than 150 KHz could be achieved in a molecular iodine beam [10.6]. At such small linewidths the time of flight broadening due to the finite interaction time of the molecules with a focussed laser beam is no longer negligible, since the spontaneous lifetime already exceeds the transit time.

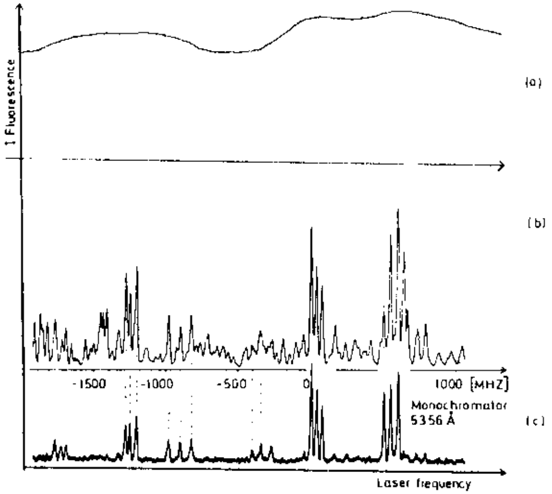

Fig.10.4a-c. Section of the excitation spectrum of NO_2 obtained with a single-mode argon laser, tunable around $\lambda = 488$ nm. (a) In an NO_2 cell ($p = 0.01$ torr), (b) in a collimated NO_2 beam with a collimation ratio of 1 : 80, (c) filtered excitation spectrum. Instead of the total fluorescence as in (b) only the (0,1,0) fluorescence band was monitored

Besides these three examples a large number of atoms and molecules have been studied in molecular beams with high spectral resolution. Mainly hyperfine structure splittings, isotope shifts, and Zeeman splittings have been investigated by this technique because these splittings are generally so small that they may be completely masked in Doppler-limited spectroscopy. An impressive illustration of the sensitivity of this technique is the measurement of nuclear charge radii and nuclear moments of stable and radioactive instable isotopes through the resolution of optical hfs splittings and isotope shifts performed by several groups [10.7-11]. Even spurious concentrations of short-lived radioactive isotopes could be measured in combination with an on-line mass separator.

More examples of sub-Doppler spectroscopy in atomic or molecular beams can be found in reviews on this field by JACQUINOT [10.11] and LANGE et al. [10.12].

10.1.2 Laser Spectroscopy in Supersonic Beams

An interesting development in the high-resolution spectroscopy of complex molecules in molecular beams takes advantage of the internal cooling of molecules in supersonic beams [10.13]. When a gas expands freely from a high-pressure region into the vacuum, adiabatic cooling of the internal energy occurs. This means that the thermal energy of the molecules in the source, which is composed of translational, rotational, and vibrational energy, is partly transferred into expansion energy. This transfer occurs during the expansion in the orifice at densities where the collision probability is high. The degree of cooling depends on the number of collisions during the expansion which is proportional to the product nd of density and orifice diameter [10.14].

Since the cross sections for elastic collisions are larger than those for collision-induced rotational transitions which are still larger than those for vibrational transitions, the translational cooling [which means a narrowing of the velocity distribution $n(v_z)$] will be more effective than the rotational or vibrational cooling. While at thermodynamic equilibrium in the oven all degrees of freedom have the same mean energy $(1/2)kT$, which implies that the translational temperature T_t equals the rotational temperature T_r as well as the vibrational temperature T_v, after the adiabatic expansion the translational energy T_t has decreased more than T_r and T_v, and we obtain at the intersection region with the laser beam

$$T_t < T_r < T_v \quad .$$

Typical values achieved for these temperatures in supersonic beams at oven pressures of some atmospheres are

$$T_t \approx 0.5\text{-}20 \text{ K} \quad , \quad T_r \approx 2\text{-}50 \text{ K} \quad , \quad T_v \approx 10\text{-}100 \text{ K} \quad .$$

This internal cooling has two definite advantages for high-resolution laser spectroscopy.

a) Because of the low values of T_r and T_v, only the lowest rotational-vibrational levels in the electronic ground state are populated. Assuming thermodynamic equilibrium within each degree of freedom, the population in a level (v,J) with vibrational quantum number v and rotational number J is given by

$$n(v,J) = \frac{2(J+1)}{N}\, e^{-(v+\frac{1}{2})\hbar\omega_e/kT_v}\, e^{-B_eJ(J+1)/kT_r} \quad , \qquad (10.11)$$

[illegible]

where $N = \sum n(v,J)$ is the total number of molecules, $v\hbar\omega_e$ the vibrational energy in level v, and $B_eJ(J+1)$ the rotational energy. [illegible]

Since the intensities of absorption lines are proportional to the population densities n(v,J) of the absorbing levels, this reduction of n(v,J) to a few populated levels implies a considerable reduction of the number of

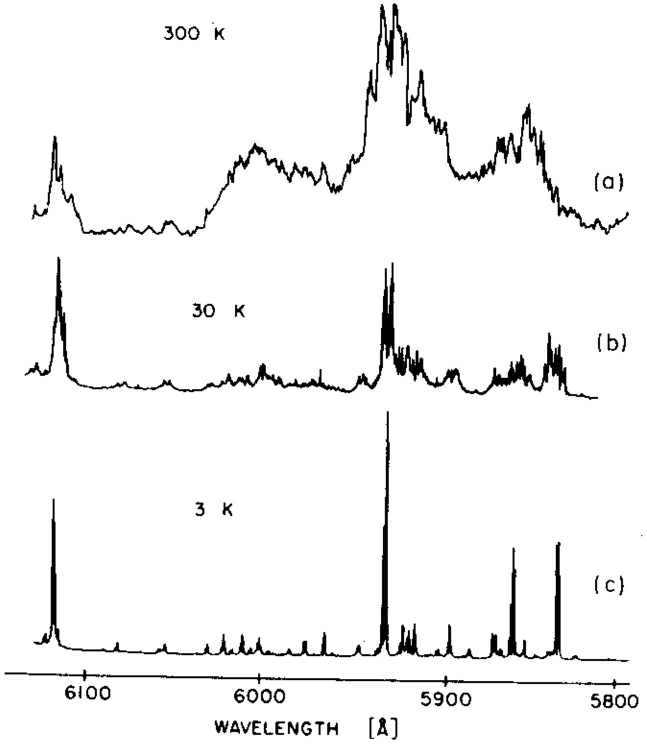

Fig.10.5a-c. Reduction of the complexity of the NO_2 excitation spectrum by internal cooling in a supersonic beam. (a) Conventional room temperature sample of pure NO_2 at 0.04 torr, (b) supersonic beam of pure NO_2, (c) supersonic beam of 5% NO_2 in Ar. The excitation source was a cw dye laser with 0.5 Å bandwidth [10.13]

absorption lines and leads to an appreciable simplification of the spectrum. This is illustrated by Fig.10.5, which shows three times the same section of the NO_2 excitation spectrum, obtained in a conventional absorption cell at room temperature, in a pure NO_2 supersonic beam with medium cooling (rotational temperature 30 K) and in a beam of argon, seeded with 5% of NO_2. Due to many collisions between the argon atoms at high density and the NO_2 molecules, the rotational temperature drops to 3 K.

b) Because of these low temperatures, loosely bound molecules with small dissociation energies D_e can be formed in supersonic beams, which would immediately dissociate at room temperature if $kT \gg D_e$. The spectroscopy of these "van der Waals molecules" opens a new area for the investigation of

interaction potentials which before could only be studied through scattering experiments. The much higher accuracy of spectroscopic measurements will improve the exact knowledge of long-range interactions, as for instance experienced by molecules in $^3\Sigma$ ground states (see below) [10.15].

This is not only important to understand the chemistry of loosely bound complexes but also contributes to elucidating molecular structure in the transition region between free molecules and solids. One example of this is the formation of clusters in supersonic alkali beams where molecules Na_x have been observed from x = 2 to x = 12 [10.16]. The spectroscopy of such multimers (clusters) yields dissociation energies, ionization energies, and vibrational structure as a function of the number x of atoms in the cluster. The comparison of these figures with the values in the solid allows the proof of theoretical models, which explain the transition from molecular orbitals to the band structure of solids.

Besides its merits for high-resolution spectroscopy the absorption spectrum in a molecular beam, generated by a tunable monochromatic laser, can be also used to measure the velocity distribution $n(v)$ of molecules in a defined level E_i at arbitrary locations in the beam. For this purpose the incident laser beam is split into two parts (see Fig.10.6a). The first beam 1 crosses the molecular beam perpendicularly while beam 2 intersects the common crossing point at an angle β with the z axis. When the laser wavelength λ is continuously tuned across a molecular absorption line, an absorption profile around the unshifted center frequency ω_0 with a reduced Doppler width is obtained from beam 1 while beam 2 produces a Doppler-shifted and Doppler-broadened absorption profile. Since each molecule which travels at a velocity $v \approx v_z$ absorbs at the Doppler-shifted frequency $\omega_0' = \omega_0 - kv\cos\beta$, the absorption profile $\alpha(\omega) = n(v\cos\beta)\sigma(\omega - \omega_0)$ of beam 2 reflects the velocity distribution $n(v)$.

From the maximum of the shifted absorption profile the most probable velocity v_p can be deduced [10.17]. Figure 10.6b illustrates the measurement of velocity distributions of Na_2 molecules in specified quantum states at different oven temperatures. The narrowing of the velocity distribution with increasing oven temperature and the increase of the most probable velocity v_p characterize the transition region from a thermal effusive molecular beam to a supersonic beam. The velocity distribution in the supersonic beam can be described by

$$n(v)dv = C\,\frac{\cos\vartheta}{r^2}\,Nv^2\,e^{-(v-u)^2/v_p^2}\,dv \;, \qquad (10.12)$$

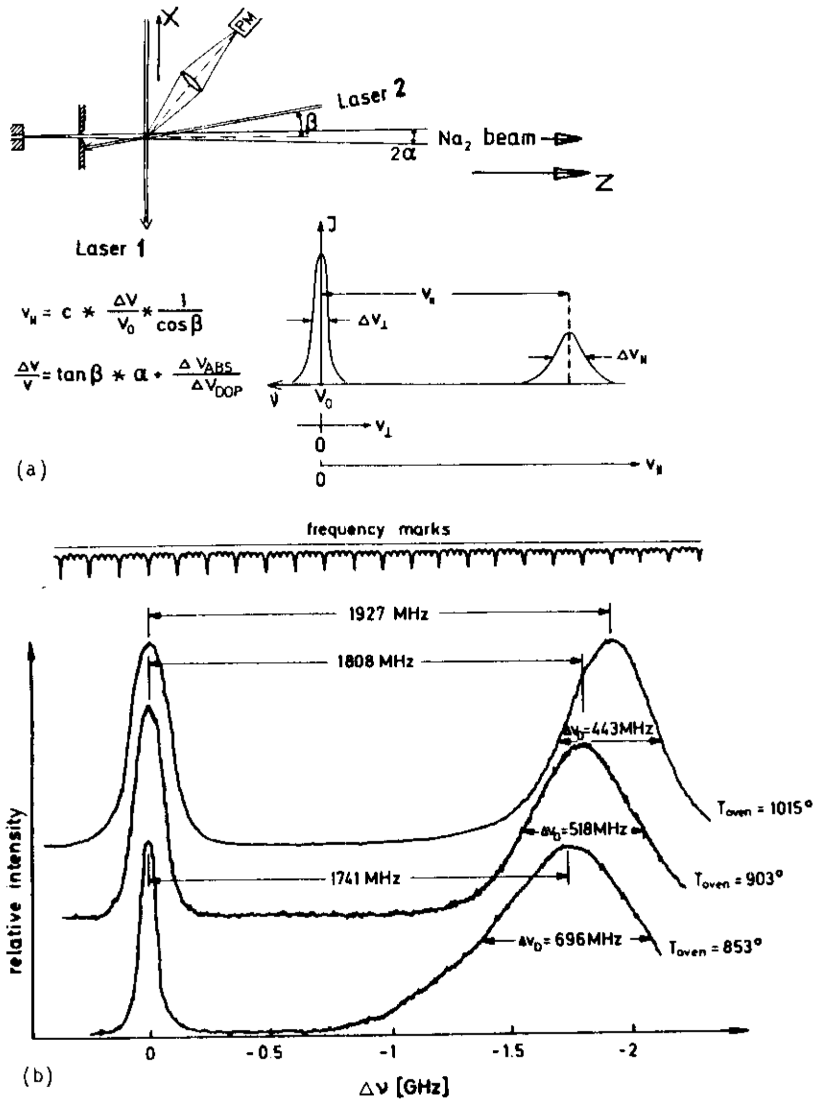

Fig.10.6a,b. Doppler shift laser spectroscopy of the velocity distributions of Na_2 molecules and their dependence on the vapor pressure p(T) in the oven. (a) Experimental arrangement, (b) velocity distributions $n(v,v''=0,J''=28)$ of molecules in the vibrational level $v''=0$ and rotational level $J''=28$ at three different oven temperatures [10.17]

where $v_p = (2kT_t/m)^{\frac{1}{2}}$ is much smaller because of the smaller translational temperature T_t. The parameter u characterizes the deviation of the supersonic distribution from a thermal distribution.

Compared with conventional methods of measuring velocity distributions with mechanical selectors or with conventional time-of-flight tubes, this spectroscopic detection method has the following advantages:

a) The accuracy of spectroscopic techniques is generally higher than that obtained with mechanical velocity selectors.

b) The velocity distribution of molecules *in selected vibrational-rotational levels* can be measured. This is of particular importance in crossed beam experiments where inelastic collision processes are studied and the transfer of energy from translational to internal energy can be detected in detail.

c) The velocity and its distribution can be measured at localized points in the beam which allows one to detect local variations of $n(v,E_i)$ along and across the beam. This gives information about the formation of molecules during the expansion and in the region where collisions still occur.

Note, that at low laser intensities the densities $n(v)dv$ are measured. However, at higher laser intensities, where complete saturation occurs, the *flux densities* $vn(v)dv$ are detected.

The relative populations $n(v_i,J_i)/(n(v_k,J_k)$ in the supersonic beam can be measured in the following way. Part of the laser beam is split into a glass cell containing Na-Na_2 vapor at thermal equilibrium. When the laser frequency is tuned through the Na_2 absorption lines, the laser-induced fluorescence both from the cell and from the crossing point of laser beam 1 with the molecular beam is monitored simultaneously. Since the fluorescence intensity at nonsaturating laser intensities is proportional to the population densities in the absorbing levels, the relative populations $n_B(v_i,J_i)/n_B(v_k,J_k)$ in the molecular beam can be obtained from the ratio of the fluorescence intensities

$$\frac{I_c(v_i,J_i)/I_c(v_k,J_k)}{I_B(v_i,J_i)/I_B(v_k,J_k)} = \frac{n_c(v_i,J_i)/n_c(v_k,J_k)}{n_B(v_i,J_i)/n_B(v_k,J_k)} \quad .$$

The population ratio in the cell at thermal equilibrium

$$\frac{n_c(v_i,J_i)}{n_c(v_k,J_k)} = \frac{g_i}{g_k}\, e^{-(E_i-E_k)/kT}$$

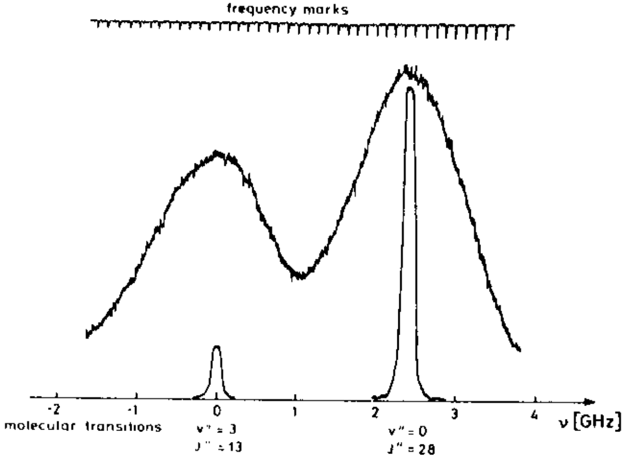

Fig.10.7. Relative population distribution of Na_2 molecules in two levels (v" = 0, J" = 28, v" = 3, J" = 43) in a thermal vapor cell at T = 500 K and in a supersonic beam

follows a Boltzmann distribution. Figure 10.7 shows as an example the Doppler-broadened line profiles from the cell and the corresponding lines with reduced Doppler width in the supersonic beam. One clearly sees that the vibrational level at v" = 3 is much less populated in the supersonic beam than in the cell, which had a temperature of about 500 K. This indicates the vibrational cooling in the beam [10.17a].

10.1.3 Laser Spectroscopy in Fast Ion Beams

In the examples considered so far, the laser beam was crossed *perpendicularly* with the molecular beam, and the reduction of the Doppler width was achieved through the limitation of the maximum velocity components V_x by geometrical apertures. One therefore often calls this reduction of the transverse velocity components "*geometrical cooling*". KAUFMANN [10.18a] and WING et al. [10.18b] have independently proposed another arrangement, where the laser beam travels *collinear* with a fast ion or atom beam and the reduction of the *longitudinal* velocity distribution $n(v_z)$ is achieved by an acceleration voltage ("acceleration cooling").

Assume that two ions start from the ion source (Fig.10.8) with different thermal velocities $v_1(0) = 0$ and $v_2(0) > 0$. After being accelerated by the voltage U their kinetic energies are

$$E_1 = e\,U = \frac{m}{2}v_1^2$$

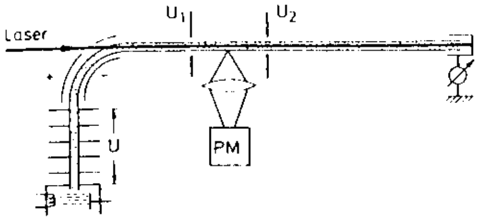

Fig.10.8. Laser spectroscopy in fast ion beams. The laser beam is *collinear* with the ion beam

$$E_2 = \frac{m}{2}v_2^2(0) + eU = \frac{m}{2}v_2^2 \quad .$$

Subtracting the first from the second equation yields

$$v_2^2 - v_1^2 = v_2^2(0) \Rightarrow \Delta v = v_2 - v_1 = v_2^2(0)/2v \quad \text{with} \quad v = (v_1 + v_2)/2 \quad .$$

This means that the initial velocity spread $v_2(0)$ has decreased to

$$\Delta v = v_2(0)\left(\frac{v_2^2(0)m}{8eU}\right)^{1/2} = v_2(0)\left(\frac{\Delta E_{th}}{4eU}\right)^{1/2} \quad . \tag{10.13}$$

Example

$\Delta E_{th} = 0.1$ eV; $eU = 10$ KeV $\Rightarrow \Delta v = 1{,}5 \times 10^{-3}\,v_2(0)$.

This reduction of the velocity spread results from the fact that *energies* rather than velocities are added. If the energy $eU \gg E_{th}$ the velocity change is mainly determined by U but hardly by the fluctuations of the initial thermal velocity. This implies, however, that the acceleration voltage has to be extremely well stabilized to take advantage from this "acceleration cooling".

A definite advantage of this parallel arrangement is the longer interaction zone between the two beams because the laser-induced fluorescence can be collected by a lens from a path length ΔZ, of several cm, compared to a few mm in the perpendicular arrangement. A further advantage is the possibility of Doppler tuning. The absorption spectrum of the ions can be scanned across a *fixed* laser frequency ω simply by tuning the acceleration voltage U. An absorption line at ω_0 is Doppler tuned into resonance with the laser field, at frequency ω, if

$$\boxed{\omega = \omega_0 - kv_z = \omega_0\left(1 - \sqrt{\frac{2eU}{mc^2}}\right)} \quad . \tag{10.14}$$

This allows one to use high-intensity fixed frequency lasers, such as the argon laser, which have a high gain and even allow one to place the interaction zone inside the laser cavity.

Instead of tuning the acceleration voltage U (which influences the beam collimation), the velocity of the ions in the interaction zone with the laser beam is tuned by retarding or accelerating potentials U_1 and U_2 (see Fig.10.8).

This superimposed ion-laser beam geometry is quite suitable for high-sensitivity spectroscopy with high resolution, as has been demonstrated by MEIER et al. [10.19] who resolved the hfs pattern of odd xenon isotopes and by OTTEN et al. [10.20] for Hg isotopes. Such a laser-ion coaxial beam spectrometer has been described in detail by HUBER et al. [10.21]. If the laser photodissociates the molecular ions, the photo-fragments can be analyzed with great efficiency. In this case the coaxial arrangement is clearly superior to the crossed beam arrangement because the interaction time of the molecular ions with the laser field can be made several orders of magnitude longer.

Figure 10.9 shows a velocity-tuned spectrum of O^+ photofragments from the process

$$O_2^+ + h\nu \rightarrow O_2^{+*} \rightarrow O^+ + O \quad .$$

The laser wavelength was kept at λ = 5815 Å and the velocity of the O_2^+ ions was continuously tuned by controlling the acceleration voltage. More examples, including saturation spectroscopy in fast ion beams, can be found in the review by DUFAY and GAILLARD [10.22].

The fast ions can be converted to neutral atoms by charge exchange collisions while passing through a target gas chamber. Since charge exchange occurs preferentially at large impact parameters the velocity change during the collisions is nearly negligible and the neutral atoms still have a rather narrow velocity distribution $n(v_z)$ [10.23]. The merits of the collinear arrangement can therefore be extended to neutral atoms and molecules.

The charge exchange collisions may result in highly excited states of the neutral species. Often the population of these excited states accumulates in metastable states with long lifetimes. This opens the possibility of performing laser spectroscopy on transitions between *excited* states. While the resonance lines, corresponding to transitions from the ground state, are for most atoms in the ultraviolet region, the transitions between *excited* states are generally in the visible to infrared range and are therefore more readily accessible to the tuning range of dye lasers.

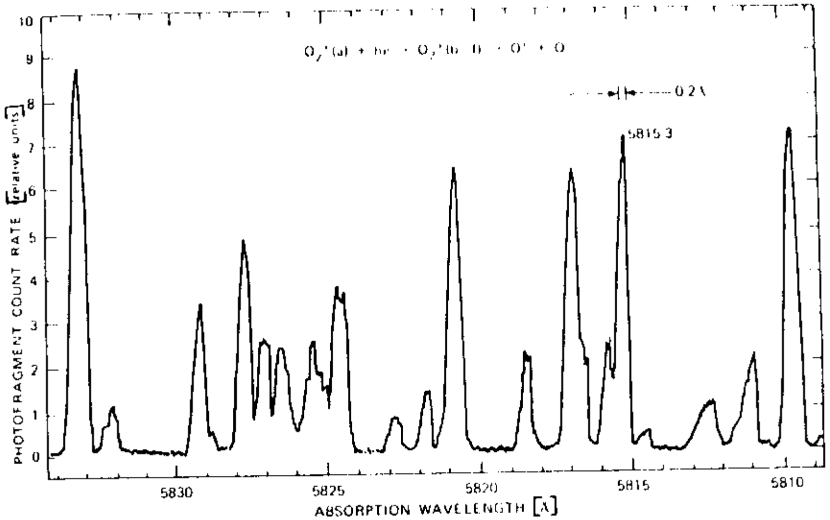

Fig.10.9. Velocity tuned spectrum of O^+-photo fragments obtained by photodissociation of O_2^+ in a "laser ion coaxial beam spectrometer" [10.22]

10.1.4 Optical Pumping in Molecular Beams

If the laser frequency ω is tuned to a molecular transition $(v_i'', J_i'' \rightarrow v_k', J_k')$, the molecules are excited into the upper level (v_k', J_k') where they can undergo spontaneous transitions $(v_k', J_k') \rightarrow (v_m'', J_m'')$ to many rotational-vibrational levels in the electronic ground state. Contrary to optical pumping in *atoms*, only the small fraction $\eta = (A_{ki}/\sum_m A_{km})$ of all excited molecules, determined by the spontaneous transition probabilities A_{km}, returns into the initial state (v_i'', J_i'').

In the intersection region of laser beam and molecular beam the pressure is already sufficiently low to exclude collisional transitions from (v_m'', J_m'') $\rightarrow (v_k'', J_k'')$. The radiative transition $(v_k', J_k') \rightarrow (v_i'', J_i'')$ is therefore the only relaxation process in diatomic homonuclear molecules which can repopulate the level (v_i'', J_i'') depleted by optical pumping. The mean recycling time for this repopulation process depends on the absorption rate $B_{ik}\rho_{ik}$ and on the spontaneous lifetime τ_k of the excited level. For $B_{ik}\rho_{ik} \gg A_k = 1/\tau_k$ one pump cycle $(i \rightarrow k \rightarrow i)$ takes a time of about τ_k. The number of pump cycles is determined by the ratio T_f/τ_k of time-of-flight T_f through the laser beam to spontaneous lifetime τ_k. Assuming a diameter of the focussed laser beam of about 0.1 mm and a mean molecular velocity $\underline{v} = 5 \times 10^4$ cm/s, we obtain

$T_f \approx 2\times10^{-7}$ s. At a spontaneous lifetime $\tau_k = 10^{-8}$ s this implies that about 20 pump cycles are possible. With a value of $\eta = 0.1$ the population of the pumped level (v_i'', J_i'') decreases after each cycle to 10% which means that after 2 pump cycles the population has already dropped to about 1% of its unsaturated value.

This illustrates that optical pumping in molecular beams is a very efficient way to completely deplete a specified molecular level (v_i'', J_i''). This can be used to gain detailed information on velocity distributions in supersonic beams of molecules in defined quantum states and on relaxation processes, molecular formation, and collision processes in crossed molecular beams.

The following is an example of one of the many possible applications of optical pumping to a time-of-flight spectrometer with velocity selection for molecules in defined quantum states in supersonic beams [10.24].

The monochromatic laser beam is split into two beams 1 and 2, both of which cross the molecular beam perpendicularly but at different locations $z_1 = A$ and $z_2 = B$ (see Fig.10.10). When the laser frequency is tuned to a molecular transition $(v_i'', J_i'' \rightarrow v_k', J_k')$, the molecules passing through the pump beam 1 are optically pumped and there are nearly no molecules left in the depleted level (v_i'', J_i''). This means that the fluorescence excited by the probe beam 2 is very low. If the pump beam 1 is interrupted for a short time interval Δt (e.g., by a fast mechanical chopper) the molecules can pass during this interval Δt without being pumped. Because of their different velocities they reach the probe beam 2 at different times $t = L/v$, where $L = z_2 - z_1$. The time-resolved fluorescence intensity induced by the cw probe beam therefore reflects the velocity distribution of molecules in the level (v_i'', J_i''). Figure 10.11 shows for the case of Na_2 molecules in a supersonic beam that these velocities are *different* for different quantum states. This has to do with the fact that during the adiabatic expansion in the nozzle the internal energy of the molecules is partly converted into expansion energy and the expansion velocity depends on the degree of energy transfer a molecule has suffered [10.24a].

10.1.5 Optical-Optical Double-Resonance Spectroscopy in Molecular Beams

This selective depletion of specified rotational-vibrational levels by optical pumping can also be used to facilitate the identification of complex molecular spectra. The basic concept is illustrated in Fig.10.12. Differing from Fig.10.10 the pump beam and the probe beam come from two different

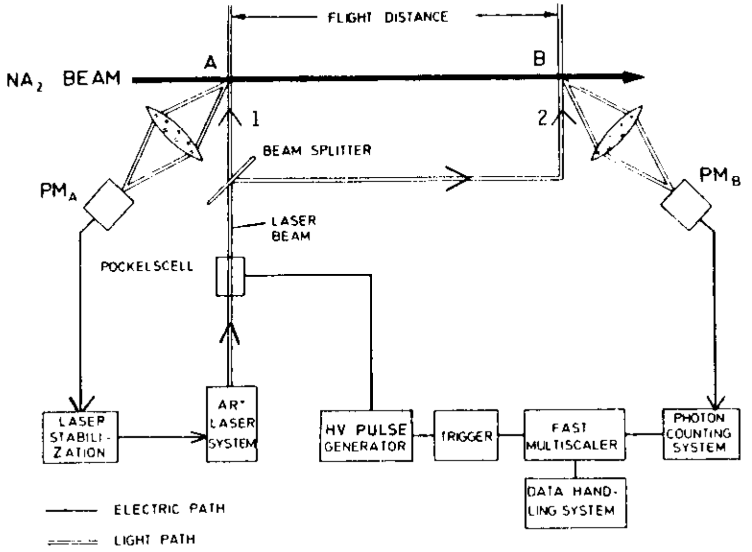

Fig.10.10. Optical time-of-flight spectrometer for the determination of velocity distributions $n_i(v_z)$ of molecules in defined quantum states (v_i, J_i)

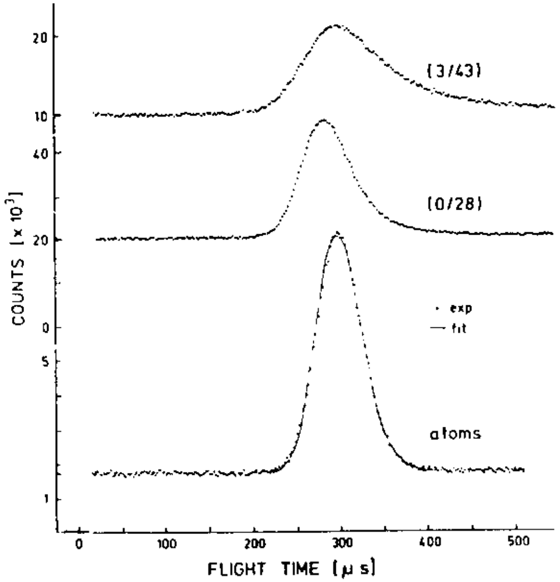

Fig.10.11. Time-of-flight spectrum of Na_2 molecules in two different quantum states ($v'' = 3$, $J'' = 43$) and ($v'' = 0$, $J'' = 28$) in comparison with the Na atom velocity distribution [10.24]

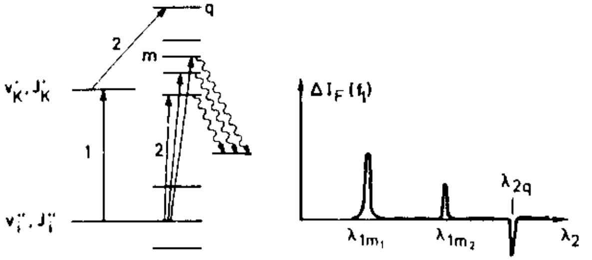

Fig.10.12. Labeling of specified upper or lower levels (v,J) by optical pumping and successive probing (optical-optical double resonance)

lasers. If the pump laser 1 which is stabilized onto the molecular transition $(v_i'',J_i'') \rightarrow (v_k',J_k')$ is chopped at the frequency f_1, the population densities n_i and n_k are also chopped, where the phase of $n_i(f_1)$ is opposite to that of $n_k(f_1)$. If the wavelength λ of the unchopped probe laser 2 is tuned across the absorption spectrum of the molecules, the laser-induced fluorescence intensity I_{Fl} which is proportional to n_iI_2 or n_kI_2, respectively, will always be modulated at f_1 if the probe laser hits a transition which starts from one of the optically pumped levels E_i or E_k. The modulation phase is opposite for the two cases. When the fluorescence is detected through a lock-in amplifier, tuned to the chopping frequency f_1, only those of the many possible transitions induced by the tunable probe laser are detected that are connected to one of the pumped levels E_i or E_k (see Fig.10.12b).

This optical-optical double-resonance technique has already been used for other Doppler-free techniques [10.25], such as polarization spectroscopy (see Sect.10.3). Its applications to molecular beams has, however, the following advantages compared to spectroscopy in gas cells. When the chopped pump laser periodically depletes the level E_i and populates level E_k, there are two relaxation mechanisms in gas cells which may transfer the population modulation to other levels. These are collision processes and laser-induced fluorescence (see Fig.8.39). The neighboring levels therefore also show a modulation and the modulated excitation spectrum induced by the probe laser includes all lines which are excited from those levels. If several absorption lines overlap within their Doppler width, the pump laser simultaneously excites several upper states and also partly depletes several lower levels. The simplification and the unambiguous assignment of the lines is therefore partly lost again. However, in the molecular beam, Doppler-free excitation is possible and collisions can be neglected. Since the fluorescence from the excited level E_k terminates on *many* lower levels (v_m'',J_m''), only a small frac-

10

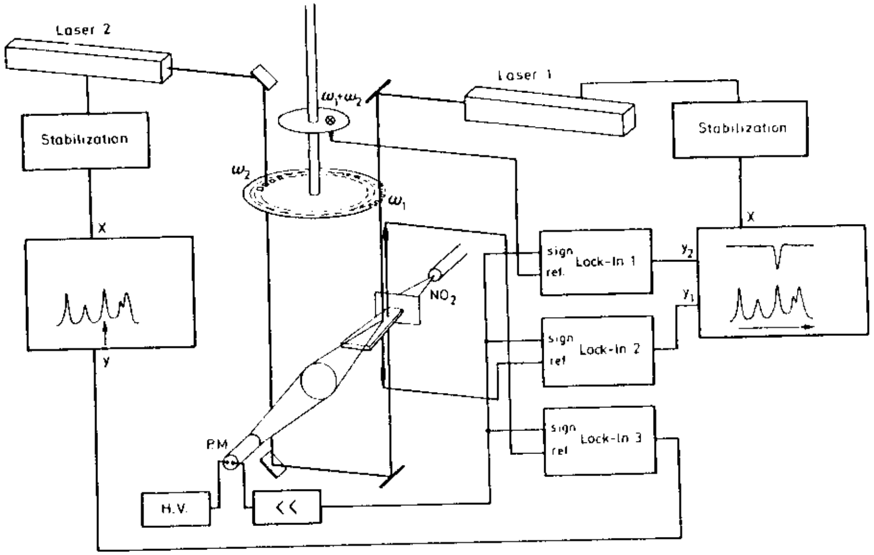

Fig.10.13. Experimental arrangement for optical-optical double resonance in molecular beams

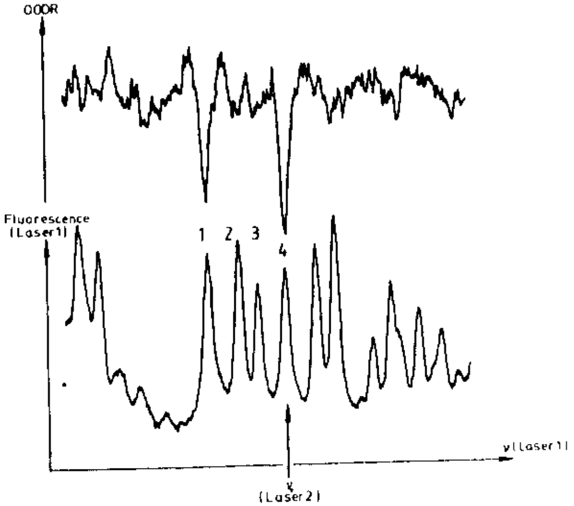

Fig.10.14. Section of linear NO_2 spectrum around λ = 488 nm (lower trace) and double-resonance spectrum (upper trace). The pump laser was stabilized on line No. 4 while the probe laser was tuned [10.26]

tion of the population n_i from the depleted level E_i is pumped into each of the levels E_m which are populated by fluorescence decay from E_k. This means that the modulation amplitude is much smaller if the probe laser is tuned to levels E_m rather than to E_i.

Molecules with long spontaneous lifetimes may fly several centimeters before they radiate and may therefore emit their modulated fluorescence at the location of the probe beam. In order to distinguish this modulated fluorescence from that excited by the probe laser, both lasers are chopped at two different frequencies f_1 and f_2. The fluorescence intensity excited by the probe laser tuned to the transition $(v_i'',J_i'') \rightarrow (v_m,J_m)$ is then

$$I_{Fl}(I_2) \propto N_i I_2 = (N_{i0} - aI_1)I_2$$

$$= [N_{i0} - aI_{01}(1 - \cos 2\pi f_1 t)]I_{02}(1 - \cos 2\pi f_2 t)$$

and therefore contains terms with the sum frequency $(f_1 + f_2)$. Tuning the detection system to $(f_1 + f_2)$ therefore selects those transitions which are due to transitions excited by the probe laser from a level E_i which had been depleted by laser 1. Figure 10.13 shows the experimental arrangement. Figure 10.14 compares a section of the linear excitation spectrum of NO_2 with the double-resonance spectrum detected at $(f_1 + f_2)$ where the pump laser 1 had been stabilized to line No. 4. The double resonance spectrum shows that lines No. 1 and 4 share the same lower level [10.26], information which could not have been deduced easily from the linear spectrum.

10.1.6 Radio-Frequency Spectroscopy in Molecular Beams

The "Rabi technique" of radio-frequency or microwave spectroscopy in atomic and molecular beams [10.27a] has made an outstanding contribution to the accurate determination of ground state parameters, such as the hfs splittings in atoms and molecules or the Coriolis splittings in molecules, etc. Figure 10.15 depicts schematically a conventional Rabi beam apparatus. Molecules with a permanent dipole moment μ effuse from the orifice of the oven and are collimated by the slit S_1. In an inhomogeneous magnetic field (A field) they experience a force $\underline{F} = -\underline{\mu}$ grad $\underline{B}$ and are therefore deflected. In a second reversed inhomogeneous field (B field) they experience an opposite force and are therefore deflected back onto the detector. If an rf field in a homogeneous field region C between the A and the B field induces transitions to other molecular levels the dipole moment $\underline{\mu}$ changes and the B field does not deflect the molecules exactly back onto the detector. This means that the detected beam intensity $I(\nu_{rf})$ as a function of the radio frequency ν_{rf} shows a dip in case of resonance. Because of the long spontaneous lifetimes in electronic ground states the linewidth of this dip is mainly determined by the time of flight through the rf field and by saturation broadening [10.27b].

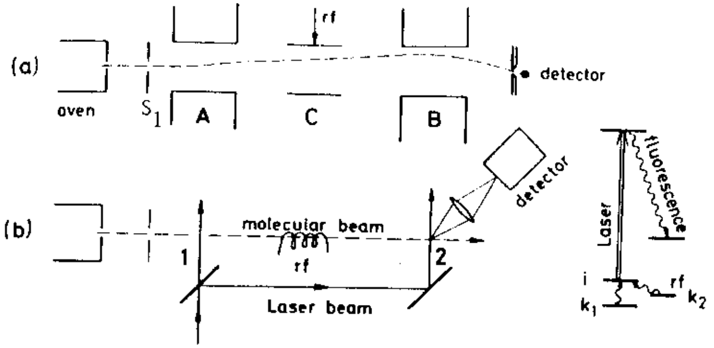

Fig.10.15. Comparison between conventional Rabi method (a) and its laser equivalent (b)

Optical pumping with lasers offers a new and very convenient variation of the conventional Rabi method, which is illustrated in Figs.10.15b and 10.16. The two inhomogeneous magnetic fields A and B are replaced by two parallel laser beams which cross the molecular beam perpendicularly. The first "pump beam" depletes the population N(i) of the lower level i. This is monitored by the resultant decrease of the fluorescence intensity I_{Fl} induced by the probe laser. When the rf field induces transitions k → i between other levels k and the depleted level i, the population N(i) is increased, resulting in a corresponding increase of I_{Fl}.

The laser version of the Rabi method does not rely on the mechanical deflection of molecules but uses the change of the population density in specified levels due to optical pumping. The conventional technique is restricted to atoms or molecules with magnetic or electric dipole moments and the sensitivity depends on the difference between the dipole moments in the two levels connected by the rf transition. The laser version can be applied to all atoms and molecules which can be optically pumped by existing lasers. The background noise is small because only those molecules which are in the specified level contribute to the probe-induced fluorescence.

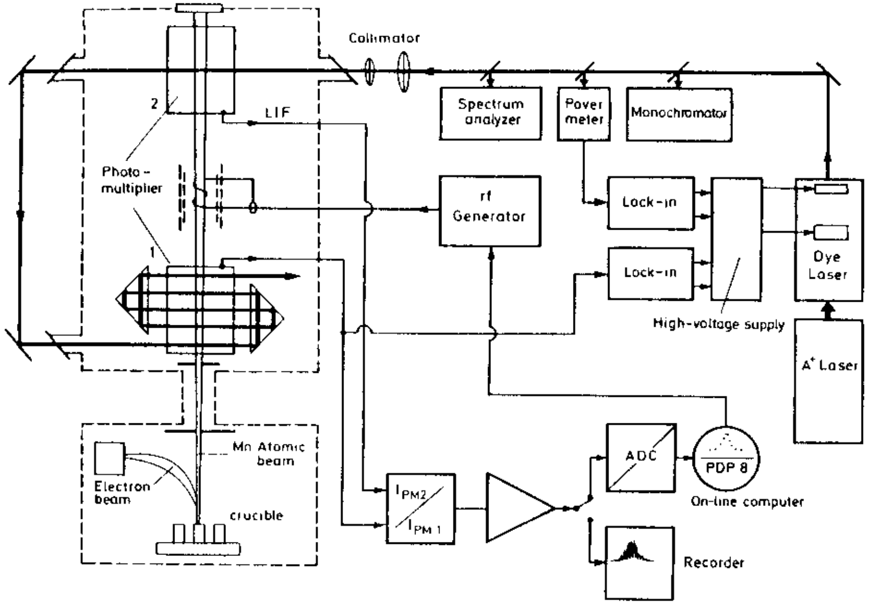

Fig.10.16. Schematic diagram of atomic beam magnetic resonance method using optical pumping and probing with lasers [10.27e]

Some examples illustrate the achievable sensitivity and accuracy: ERTMER and HOFER [10.27c] measured the hyperfine structure of metastable states of scandium which were populated by electron impact. The population achieved in these states was only about 1% of the ground state population. Optical pumping to a higher electronic state with a single-mode dye laser allowed selective depletion of the single hfs sublevels of the metastable F state. The hfs constants could be determined with an accuracy of a few kHz.

ROSSNER et al. [10.27d] measured the very small hfs splitting (< 100 kHz) of a rovibronic level ($v'' = 0$, $J'' = 28$) in the X $^1\Sigma_g$ ground state of the Na_2 molecule. This splitting is much smaller than the natural linewidth of the optical transitions. The quadrupole coupling constant was determined to $e\,q\,Q = 463.7 \pm 0.9$ kHz and the nuclear spin-molecular rotation interaction constant came out to be $a = 0.17 \pm 0.03$ kHz.

Figure 10.16 shows a block diagram of the whole apparatus, used by PENSELIN and his group for atomic beam magnetic resonance spectroscopy detected by laser-induced fluorescence [10.27e]. The pump laser beam crosses the atomic beam several times to assure high pumping efficiency. The rf transitions induce population changes, which are detected by the laser-induced fluorescence in the probe region. For further examples see [10.27f].

10.2 Saturation Spectroscopy

Saturation spectroscopy is based on the selective saturation of an inhomogeneously broadened molecular transition by optical pumping with a monochromatic tunable laser. As has been outlined in Sect.3.6 the population density $n_i(v_z)dv_z$ of molecules in the absorbing state E_i is selectively depleted of molecules with velocity components

$$v_z \pm dv_z = (\omega_0 - \omega \pm \delta\omega)/k$$

in the interval dv_z, because these molecules are Doppler shifted into resonance with the laser frequency ω and are excited from E_i to the higher level E_k ($E_k - E_i = \hbar\omega_0$).

The monochromatic laser therefore "burns a hole" into the population distribution $n_i(v_z)$ of the absorbing state and produces simultaneously a peak at the same velocity component v_z in the upper state distribution $n_k(v_z)$ (Fig.10.17).

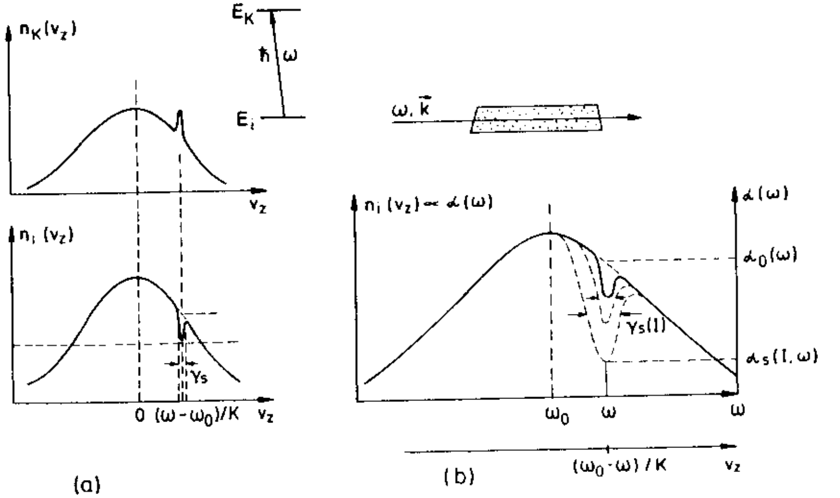

Fig.10.17. (a) "Hole burning" in the lower level population distribution $n_i(v_z)$ of an absorbing transition and generation of a corresponding population peak in the upper level. (b) Increase of Bennet hole width with increasing saturating intensity

Because of this population depletion the absorption coefficient $\alpha(\omega) = \Delta n(v_z)\sigma_{ik}(\omega_0 - \omega - v_z \cdot k)$ *decreases* from its unsaturated value $\alpha_0(\omega)$ to the saturated value

$$\alpha_s(\omega) = \alpha_0(\omega)/\sqrt{1 + S_0} \tag{10.15}$$

as has been shown in (3.81a).

$\Delta n = n_i - (g_i/g_k)n_k$ gives the population difference between the two levels E_i and E_k.

$S_0 = S(\omega_0)$ is the saturation parameter at the line center (3.70) and $S = B_{ik}\rho_{ik}(\omega)/R$ is the ratio of the depleting absorption rate $B_{ik}\rho(\omega)$ to the sum R of all relaxation processes which refill the depleted level E_i.

Because the intensity absorbed over a path length dz

$$dI(\omega) = \alpha_s(\omega)I_0(\omega)dz = \alpha_0 I_0/\sqrt{1 + aI_0}\ dz \quad \text{with} \quad a = 2B_{ik}/(c\pi\gamma R) \tag{10.16}$$

is no longer linearly dependent on the incident intensity I_0, spectroscopic methods based on saturation effects are often called *nonlinear spectroscopy*.

We now briefly discuss the basic concepts and experimental arrangements of saturation spectroscopy and show that this technique allows essentially Doppler-free spectral resolution.

10.2.1 Basic Concepts

Assume that a monochromatic laser wave $E = E_0 \cos(\omega t - kz)$ is travelling in the +z direction through a gaseous sample with molecules at thermal equilibrium. The absorption cross section $\sigma_{ik}(\omega)$ of a molecule in level E_i that moves with velocity v is, according to (2.73) and (3.76),

$$\sigma_{ik}(\omega, v_z) = (\hbar\omega/c)B_{ik}g(\omega_0 - \omega - kv_z) \quad , \tag{10.17}$$

where the function

$$g(\omega_0 - \omega - kv_z) = \frac{\gamma_s/2\pi}{(\omega_0 - \omega - kv_z)^2 + (\gamma_s/2)^2} \tag{10.18}$$

represents the normalized homogeneous line profile of the molecular transition with $\hbar\omega_0 = (E_k - E_i)$ [see (3.10)].

The homogeneous linewidth

$$\gamma_s = \gamma\sqrt{1 + S_0} \quad \text{with} \quad \gamma = \gamma_n + \gamma_c \tag{10.19}$$

is determined by the natural linewidth γ_n, the collisional broadening γ_c, and by saturation broadening (see Chap.3). At sufficiently low pressures and small laser intensities, pressure broadening and saturation broadening may be neglected and the homogeneous linewidth γ_s approaches the natural linewidth γ_n, provided the interaction time of the molecules with the radiation field is longer than the spontaneous lifetime, so that time-of-flight broadening can be neglected (see Sect.3.4). In the visible region γ_n is several orders of magnitude smaller than the Doppler width $\Delta\omega_D$.

Since $g(\omega_0 - \omega - kv_z)$ has its maximum for $\omega_0 - \omega = kv_z$, those molecules with velocity components $v_z = (\omega_0 - \omega)/k$ have the largest absorption probability. This implies that a hole centered at $v_z = (\omega_0 - \omega)/k$ appears in the population distribution $n(v_z)$ (Fig.10.17) with a width γ_s and a depth depending on the saturation parameter S_0 at $\omega = \omega_0$. According to (3.77b) the difference $\Delta n_0(v_z) = n_i(v_z) - (g_i/g_k)n_k(v_z)$ decreases to its saturated value

$$\Delta n_s(v_z)dv_z = \Delta n_0(v_z)\left(1 - \frac{(\gamma/2)^2 S_0}{(\omega_0 - \omega - kv_z)^2 + (\gamma_s/2)^2}\right)dv_z \tag{10.20}$$

$$= C\Delta N_0\left(1 - \frac{(\gamma/2)^2 S_0}{(\omega_0 - \omega - kv_z)^2 + (\gamma_s/2)^2}\right)e^{-(v_z/v_p)^2}\ dv_z$$

with $v_p = (2kT/m)^{\frac{1}{2}}$ and $\Delta N_0 = \int \Delta n_0(v_z)dv_z$.

The spectral width γ_s of this "*Bennett hole*" [10.28] represents the homogeneous linewidth of the molecular transition and is, as mentioned above, in the visible region for $\gamma_s \rightarrow \gamma_n$ very much smaller than the Doppler width (see the examples in Chap.3).

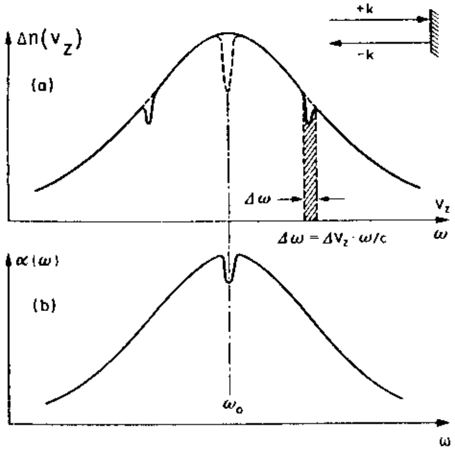

Fig.10.18. (a) Bennet hole burned symmetrically into the velocity distribution $n(v_z)$ by two counterpropagating waves of frequency $\omega \neq \omega_0$. (b) Lamb dip at the center $\omega = \omega_0$ of a Doppler-broadened absorption line $\alpha(\omega)$

In order to detect this Bennet hole, which has been burned into the population distribution $n_i(v_z)$ by the so-called *pump wave*, a second light wave, called the *probe wave* has to be sent through the sample to probe the population depletion in the hole. This probe wave may be either split from the same laser which provides the pump wave, or it may also come from another laser.

In a simple arrangement the pump wave may be reflected by a mirror back into the sample (Fig.10.18a). Since the reflected wave $E = E_0 \cos(\omega t + kz)$ has the opposite wave vector $-\underline{k}$, it interacts with another group of molecules centered around $-v_z$. As long as $\omega \neq \omega_0$, therefore two different holes at $v_z = \pm(\omega_0 - \omega)/k$ are burned into the population distribution $n_i(v_z)$ (Fig.10.18), which merge together at the line center $v_z = 0$ for $\omega \to \omega_0$ (dotted curve). The superposition of the two counterpropagating waves $E = E_0 \cos(\omega t - kz) + E_0 \cos(\omega t + kz) = 2E_0 \cos\omega t \cos kz$ represents a standing wave field. The crucial point is now that the absorption in this field (which means the total absorption of both counterrunning waves) *has a minimum for* $\omega = \omega_0$. In this case namely both waves interact with the *same molecules*, which are therefore exposed to twice the intensity. This means that the saturation parameter S becomes twice as large and the depletion of $\Delta n(v_z = 0)$ therefore is larger for $v_z = 0$ than for $v_z \neq 0$ [see (10.20) and Fig.10.18b].

To be more quantitative let us calculate the absorption coefficient $\alpha(\omega)$ in the standing wave field. According to (2.68) we can use the relation $\alpha(\omega) = \Delta N\sigma(\omega)$ and obtain

$$\alpha_s(\omega) = \int \Delta n_s(v_z)[\sigma(\omega_0 - \omega - kv_z) + \sigma(\omega_0 - \omega + kv_z)]dv_z \quad , \tag{10.21}$$

where the population difference $\Delta n(v_z)$, saturated in the standing wave, is according to (10.20) given by

$$\Delta n_s(v_z) = \Delta n_0(v_z)\left[1 - \frac{(\gamma/2)^2 S_0}{(\omega_0 - \omega - kv_z)^2 + (\gamma_s/2)^2} - \frac{(\gamma/2)^2 S_0}{(\omega_0 - \omega + kv_z)^2 + (\gamma_s/2)^2}\right] . \tag{10.22}$$

Equation (10.21) can be solved in the weak field approximation for $S_0 \ll 1$. After some elaborate calculations (see [10.53]) one obtains

$$\alpha_s(\omega) = \alpha_0(\omega)\left[1 - \frac{S_0}{2}\left(1 + \frac{(\gamma_s/2)^2}{(\omega - \omega_0)^2 + (\gamma_s/2)^2}\right)\right] . \tag{10.23}$$

This is a Doppler profile $\alpha_0(\omega) = CN_0 \exp-[(\ln 2)(\omega - \omega_0)^2/\delta\omega_0^2]$ modified by the expression in brackets, which represents a small dip at the center (Fig.10.18b) which is called *Lamb dip*, after W.E. Lamb, who first described this effect in the approximation of weak saturation [10.29].

The Lamb dip profile is Lorentzian with a halfwidth γ_s(FWHM). At the line center $\alpha_s(\omega_0)$ decreases to $\alpha_0(\omega_0)(1 - S_0)$, far off resonance to $\alpha_0(\omega)(1 - S_0/2)$. This is because for $\omega = \omega_0$ the molecules are saturated by twice the intensity, while for $\omega - \omega_0 > \gamma$ both fields interact with different molecules.

The Lamb dip in the distribution $\Delta n(v_z)$ of the population difference $\Delta n = n_1 - (g_1/g_2)n_2$ appears not only in the inhomogeneously broadened *absorption* profile $\alpha(\nu)$ but in case of inversion ($\Delta n < 0$) also in the gain profile $-\alpha(\omega)$ of an amplifying medium with an inhomogeneous linewidth. If the frequency of a single-mode gas laser is tuned over the Doppler-broadened gain profile, the output intensity shows a dip around the center frequency ω_0 [10.30]. This Lamb dip in the laser output can be used to stabilize the laser frequency to the center of the gain profile (see below).

10.2.2 Doppler-Free Saturation Spectroscopy

The narrow Lamb dips in the Doppler-broadened absorption coefficient $\alpha(\omega)$, as seen by a monochromatic standing wave, can be used to resolve closely spaced absorption lines, which would be completely masked in Doppler-limited spectroscopy. Figure 10.19 gives an example for two transitions, between hyperfine components of two molecular states, which are separated by less than their Doppler width. Although the Doppler-broadened line profiles completely overlap, their Lamb dips can be clearly resolved. The detection of these narrow resonances can be realized with different experimental arrangements, which will be discussed in the following.

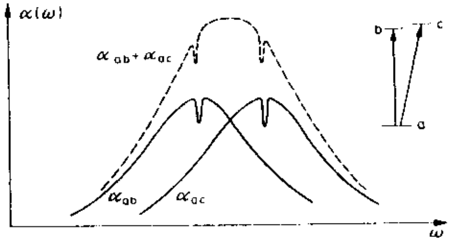

Fig.10.19. Resolution of the Lamb dips of two closely spaced transitions with overlapping Doppler profiles

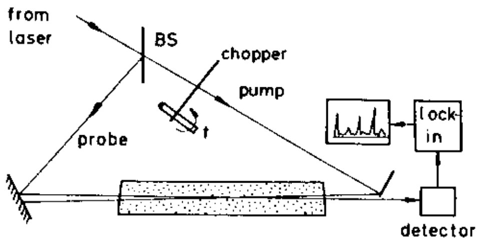

Fig.10.20. Possible experimental arrangement for saturation spectroscopy outside the laser resonator

A typical example for a possible experimental setup is shown in Fig.10.20. The output beam from a tunable laser is split by the beam splitter BS into a strong pump beam and a weak probe beam, which pass through the absorbing sample in opposite directions. The attenuation of the probe beam is measured as a function of the laser frequency ω. To enhance the sensitivity, the probe beam can be again split into two parts. One beam passes the region of the sample which is saturated by the pump beam the other passes the sample cell at an unsaturated region (see Fig.10.46). The difference of the two probe beam outputs yields the saturation signal. Figure 10.21 illustrates a saturation spectrum of the H_α line in atomic hydrogen [10.31] obtained in a hydrogen discharge with a pulsed narrow-band dye laser with a linewidth of about 7 MHz (see Sect.7.3). While the fine structure of the H_α line ($2S \rightarrow 3P$) is masked in Doppler-limited spectroscopy, a spectral resolution of 30 MHz could be achieved with saturation spectroscopy. Absolute wavelength measurements of the strong $2P_{3/2} - 3D_{5/2}$ component provided a new tenfold improved value of the Rydberg constant [10.31].

The two transitions $2S_{1/2} \rightarrow 3P_{1/2}$ at ω_1 and $2S_{1/2} \rightarrow 3P_{3/2}$ at ω_2 share a common lower level. In such cases a "crossover resonance" is observed at a laser frequency $\omega_c = (\omega_1 + \omega_2)/2$, if the Doppler width $\delta\omega_D$ is larger than $(\omega_1 - \omega_2)$. At the frequency ω_c the pump beam interacts with atoms which are Doppler-shifted into resonance on transition 1. The same atoms are then in resonance on transition 2 with the counterpropagating probe beam. Such crossover signals, which appear exactly at the mean frequency of two coupled transitions, can help to assign transitions with a common level and to separate the upper level splittings from the lower ones.

Figure 10.22 shows an example of the saturation spectrum of a mixture of different cesium isotopes contained in a glass cell heated to about 100°C [10.32]. The hyperfine structure and the isotope shifts of the different isotopes can be derived from these measurements with high accuracy.

Instead of measuring the *attenuation* of the probe beam, the absorption can also be monitored by the laser-induced *fluorescence intensity*, which is

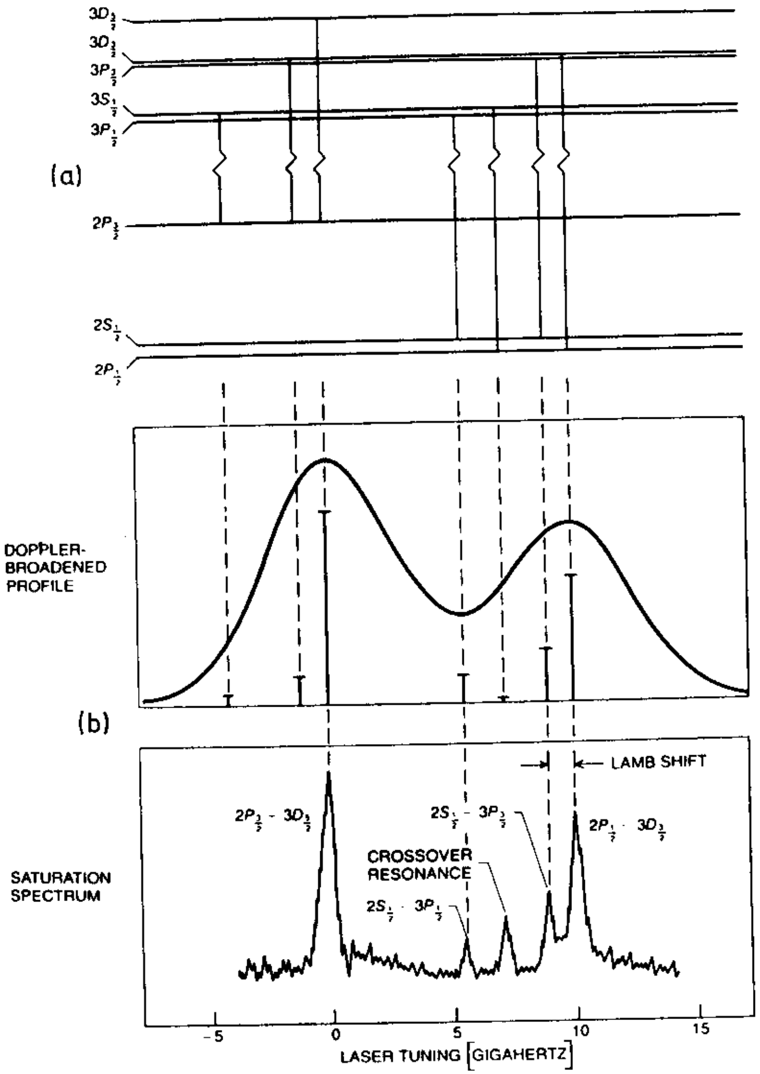

Fig.10.21a,b. Measurement of the Rydberg constant by saturation spectroscopy of the Hydrogen Balmer α transition. (a) Level scheme, (b) Doppler profiles and saturation spectrum of the Balmer α line in a hydrogen discharge [10.31a]

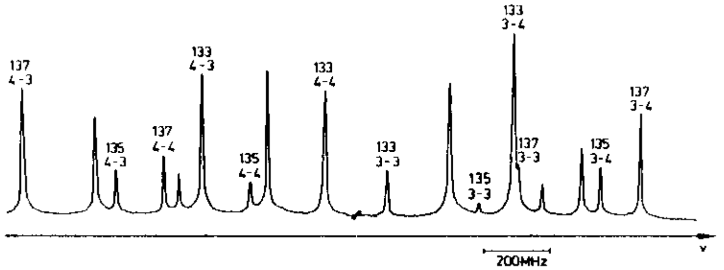

Fig.10.22. Survey scan of the saturation spectrum of all hfs components of the $6^2S_{1/2} \rightarrow 7^2P$ - transition at λ = 459.3 nm in a vapor mixture of Cs 133, 135, and 137 [10.32]

proportional to the absorbed laser intensity. In cases where the saturation is very small, the change in the attenuation of the probe beam is difficult to detect and the small Lamb dips may be nearly buried under the noise of the Doppler-broadened background. SOREM and SCHAWLOW [10.33] have demonstrated a very sensitive "intermodulated fluorescence technique", where pump beam and probe beam are chopped at two different frequencies f_1 and f_2. Assume the intensities of the two beams to be $I_1 = I_0(1 + \cos 2\pi f_1 t)$ and $I_2 = I_0(1 + \cos 2\pi f_2 t)$. The intensity of the laser-induced fluorescence is then

$$I_{Fl} = Cn_s(I_1 + I_2) \quad , \tag{10.24}$$

where n_s is the saturated population density of the absorbing state and the constant C includes the transition probabilities and the collection efficiency of the fluorescence detector. According to (10.22) the saturated population density at the center of an absorption line is $n_s = n_0(1 - S_0)$ $= n_0[1 - a(I_1 + I_2)]$.

Inserting this into (10.24) gives

$$I_{Fl} = C[n_0(I_1 + I_2) - an_0(I_1 + I_2)^2] \quad , \tag{10.25}$$

which shows that the fluorescence intensity contains linear terms, modulated at the chopping frequencies f_1 and f_2, respectively, and quadratic terms with modulation frequencies $(f_1 + f_2)$ and $(f_1 - f_2)$, respectively. While the linear terms represent the normal laser-induced fluorescence with a Doppler-broadened line profile, the quadratic terms describe the saturation effect, because they depend on the decrease of the population density $n_i(v_z = 0)$ due to the simultaneous interaction of the molecules with both fields. When the fluorescence is monitored through a lock-in amplifier, tuned to the sum frequency $f_1 + f_2$, the linear background is suppressed and only the saturation signals are detected. This is demonstrated by Fig.10.23, which shows the 15 hyperfine components of the rotational line $(v'' = 1, J'' = 98)$ $(v' = 58, J' = 99)$ in the $X^1\Sigma_g^+ \rightarrow B^3\pi_{u0}$ transition of the iodine molecule I_2 [10.34]. The two laser beams were chopped by a rotating disc with two rows of a different number of holes which interrupted the beams at $f_1 = 600\ s^{-1}$ and $f_2 = 900\ s^{-1}$. The upper spectrum was monitored at the frequency f_1 at which the pump beam was chopped while the probe was not modulated. The Doppler-broadened background caused by the linear terms in (10.25) and the Lamb-dips both show a modulation at the frequency f_1 and are therefore recorded simultaneously. The center frequencies of the hfs components, however, can be obtained more accurately from the intermodulated fluorescence spectrum (lower spectrum) which was monitored at the sum frequency $(f_1 + f_2)$ where the linear background is suppressed.

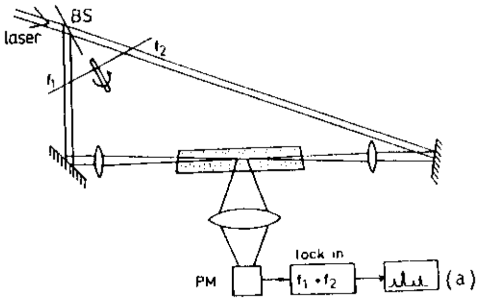

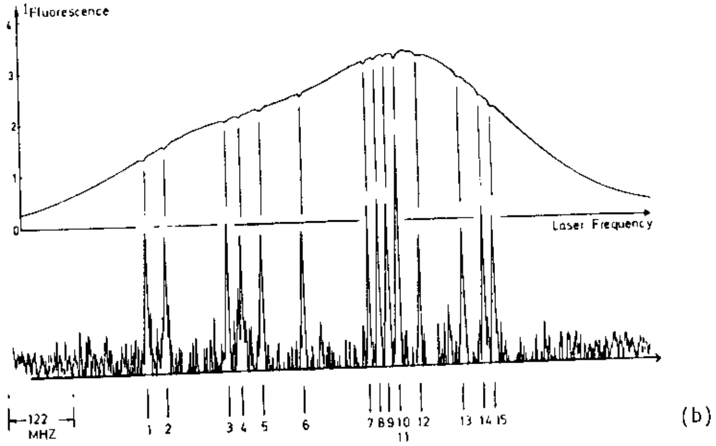

Fig.10.23a,b. Saturation spectroscopy using intermodulated fluorescence technique. (a) Experimental arrangement, (b) hyperfine spectrum of the $(v'' = 1, J'' = 98) \rightarrow (v' = 58, J' = 99)$ line in the $X^1\Sigma \rightarrow {}^3\pi_{u0}$ system of I_2 at λ = 514.5 nm, monitored at the chopping frequency f_1 of the pump beam (upper trace) and at the sum frequency (lower spectrum) [10.34]

This transition is very weak and the signal to noise ratio is therefore not very high.

Although the iodine molecule has always served as a standard example to demonstrate new sub-Doppler techniques and many papers have been published about saturation spectroscopy of I_2 [10.35], meanwhile the intermodulated fluorescence version has been applied to a number of other atoms and molecules. One example is the BO_2 molecule [10.36] where the hfs components of 37 R branch transitions involving several vibronic bands in the ground $(X^2\pi_g)$ and excited $(A^2\pi_u)$ electronic states have been resolved. For many molecules the hfs splittings are caused by two effects: an electric interaction with the electric quadrupole of a nucleus and a magnetic interaction between the nuclear spin moment and the magnetic field produced by the rotation of the molecule (spin-rotation interaction). Measuring the hfs splittings for different rotational levels allows one in many cases to separate the two contributions [10.37a,b].

Another very sensitive method of monitoring saturation signals is based on intracavity absorption. If the sample is placed inside the laser resonator, the Lamb dips in the absorption profiles represent minima of the intracavity losses. Because the laser output depends sensitively on the internal losses it will show sharp peaks when the laser frequency is tuned across the Lamb dips of the absorption profile (see Fig.10.24b).

Due to the enhancement of sensitivity in intracavity absorption (see Sect.8.2.3) these peaks in the laser output generally have a much better signal-to-noise ratio than the Lamb dips obtained with saturation spectroscopy outside the laser resonator. Furthermore, because of the nonlinear dependence of the laser output on the losses, the halfwidth of the peaks may be smaller than γ_n, particularly when the laser is operated close above threshold. Figure 10.25 illustrates such a "Lamb peak", monitored in the output of a He-Ne laser at $\lambda = 3.39$ µm with an internal methane cell [10.43]. By fortuitous coincidence an absorption line of the CH_4 molecule falls into the tuning range of the 3.39 µm laser transition. This line corresponds to a rotational line in a vibrational transition of CH_4. Because of the long lifetime of the excited vibrational level in the electronic ground state ($\tau \approx 20$ ms) the natural width γ_n of the transition is very small and the width of the Lamb dip is mainly determined by time-of-flight broadening and pressure broadening (see Chap.3). Enlarging the laser beam diameter and reducing the CH_4 pressure allows one to achieve extremely narrow resonances [10.38,39], with linewidths in the kilohertz range.

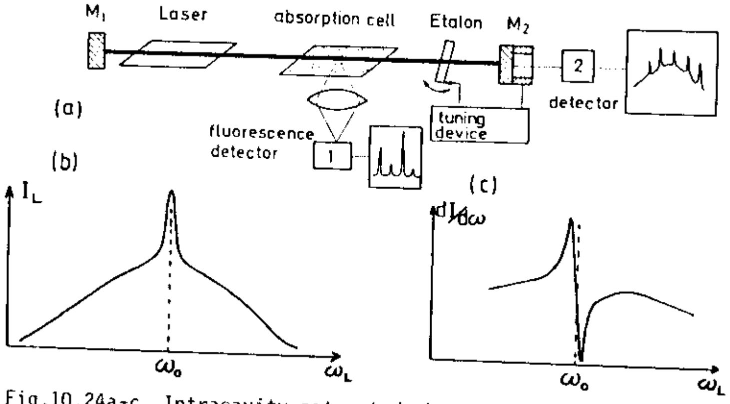

Fig.10.24a-c. Intracavity saturated absorption spectroscopy. (a) Experimental setup, (b) "Lamb peak" in the laser output, (c) derivative of a Lamb peak obtained by modulation of the laser frequency

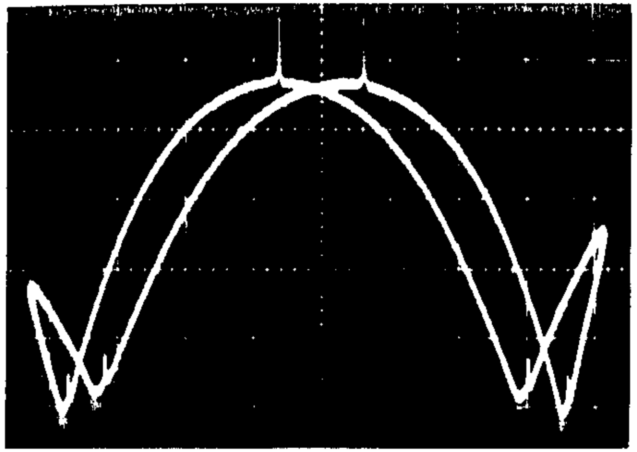

Fig.10.25. Saturation peak in the output of a He-Ne laser at λ = 3.39 nm caused by the Lamb dip of a CH_4 absorption line [10.43]. The laser frequency was swept twice over the gain profile

The sensitivity may be further enhanced by modulation of the laser frequency. This allows sensitive lock-in detection and yields signals which represent the derivative of the Lorentzian line profiles (see Sect.8.1). For illustration of the resolution achieved with extremely well-stabilized lasers, large magnifications of the laser beam diameter, and long absorption cells at low pressures, Fig.10.26 shows the modulated saturation spectrum of the $CH_3{}^{35}Cl$ molecule at $\underline{\nu} = 2947.821\ cm^{-1}$ ($\hat{=}\ \lambda = 3.39$ µm) [10.40].

Because of the chlorine nuclear spin $I = 3/2$, each rotational level with $J \geq 2$ splits into 4 hfs components with total angular momentum $\underline{F} = \underline{J} + \underline{I}$. The four lines in Fig.10.26 correspond to the four hfs transitions.

If the center frequency ω_0 of the molecular absorption line is different from the center frequency ω_1 of the gain profile $G(\omega - \omega_1)$ of the amplifying laser medium, the absorbing sample inside the laser resonator causes a Lamb peak at ω_0 in the laser output I_L, which lies at the *slope* of the gain profile (see Fig.10.27). This not only causes a slight shift of the Lamb peak center frequency, due to the sloped background, but also makes it unsafe to stabilize the laser frequency directly onto this peak. Any slight perturbation which drives the laser frequency away from the Lamb peak by more than the peak width, may induce the feedback control to drive the frequency further away to the center frequency ω_1 of the gain profile because here it also finds a zero point of the derivative $dI_L/d\omega$.

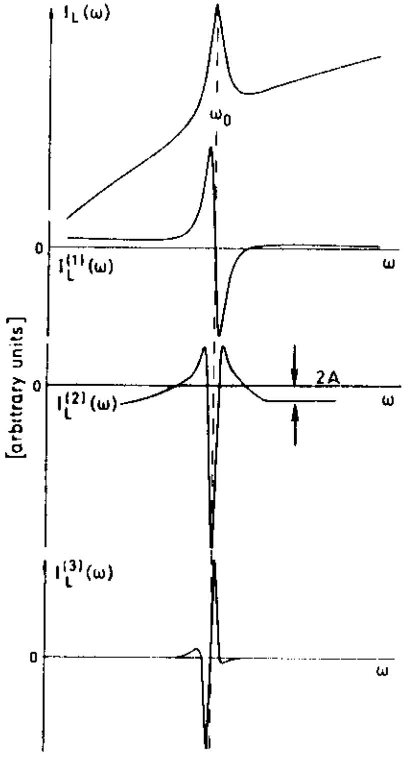

Fig.10.27. Lamb peak and its first, second, and third derivatives in the output $I_L(\omega)$ of a gas laser with intracavity absorber, when the absorption frequency ω_0 is placed at the slope of the laser gain profile

In such cases it is often advantageous to use the "*third derivative technique*" which is based on the following considerations. The frequency dependence $I_L(\omega)$ of the laser intensity is determined by the superposition of the

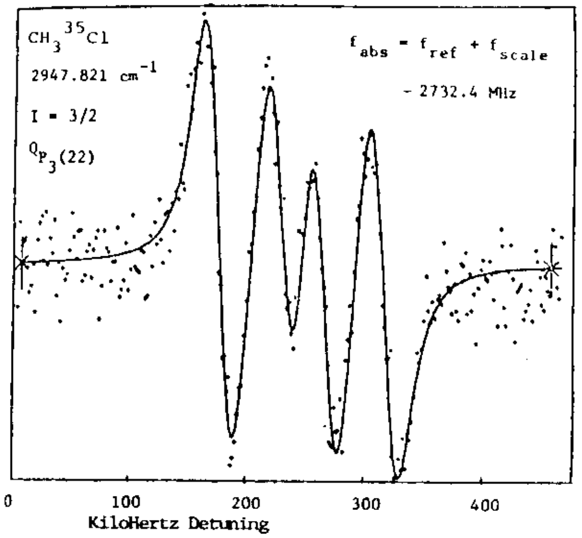

Fig.10.26. Saturated absorption spectrum of $CH_3{}^{35}Cl$ at $\lambda = 2947.821\ cm^{-1}$. The spectrum represents the derivative of four hfs components of the $^QP_3(22)$ rotational line [10.40]

10.2.3 Lamb Dip Stabilization of Gas Lasers

The extremely small linewidths, achieved with saturation spectroscopy of vibrational transitions, are not only essential for sub-Doppler resolution of closely spaced molecular lines but also allow some interesting applications in other fields of physics. One aspect is concerned with the realization of superstabilized lasers, which may serve as frequency standards in the visible or near infrared region. If the laser frequency is locked to the center of a narrow Lamb peak, its stability depends on the widths of the peak, on the signal-to-noise ratio, and on possible frequency shifts of the molecular transition caused by external perturbations, such as magnetic or electric fields, collisions, or light fields. Transitions with a small homogeneous linewidth in molecules without permanent dipole moments are therefore preferable candidates for laser stabilization. Locking the He-Ne laser at $\lambda = 0.63\ \mu m$ to a hyperfine component of a rotational line in an electronic transition of I_2 allows a frequency stability of a few kHz [10.41]. The He-Ne laser transition at $\lambda = 3.39\ \mu m$ can be locked to the vibrational transition of the CH_4 molecule even with a stability of $\Delta\nu/\nu \leq 10^{-13}$ [10.42].

gain profile $G(\omega - \omega_1)$, and the Doppler-broadened absorption profile of the absorbing probe inside the cavity with the Lamb dip at ω_0.

$$I_L(\omega) \propto \left[G(\omega - \omega_1) - \alpha_0(\omega)\left(1 - \frac{\gamma S_0}{(\omega - \omega_0)^2 + (\gamma/2)^2}\right)\right] \quad . \tag{10.26}$$

In a small interval around ω_0 we may approximate the Doppler profiles of $G(\omega - \omega_1)$ and $\alpha_0(\omega)$ by a quadratic function and obtain for (10.26) the approximation

$$I_L(\omega) = A\omega^2 + B\omega + C + \frac{D}{(\omega - \omega_0)^2 + (\gamma/2)^2} \quad , \tag{10.27}$$

where the constants A, B, C, D depend on ω_0, ω_1, γ, and S. The derivatives $I_L^{(n)}(\omega) = [(d^n I_L)(\omega)/d\omega^n]$ are

$$\begin{aligned} I_L^{(1)}(\omega) &= 2A\omega + B - \frac{2D(\omega - \omega_0)}{[(\omega - \omega_0)^2 + (\gamma/2)^2]^2} \\ I_L^{(2)}(\omega) &= 2A + \frac{6D(\omega - \omega_0)^2 - D\gamma^2/2}{[(\omega - \omega_0)^2 + (\gamma/2)^2]^3} \\ I_L^{(3)}(\omega) &= + \frac{4D\gamma^2(\omega - \omega_0)}{[(\omega - \omega_0)^2 + (\gamma/2)^2]^4} \quad . \end{aligned} \tag{10.28}$$

These derivatives are shown in Fig.10.27 which demonstrates that the Doppler-broadened background disappears for the higher derivatives. It is therefore advantageous to stabilize the laser frequency ω_L to the zero point ω_0 of the third derivative. This can be performed as follows.

If the laser frequency ω_0 is modulated at a frequency Ω, the laser intensity

$$I_L(\omega) = I_L(\omega_0 + a \sin\Omega t)$$

can be expanded into a Taylor series around ω_0

$$\begin{aligned} I_L(\omega) = I_L(\omega_0) & \\ & + a \sin\Omega t I_L^{(1)}(\omega_0) \\ & + \frac{a^2}{2} \sin^2\Omega t \, I_L^{(2)}(\omega_0) \\ & + \frac{a^3}{6} \sin^3\Omega t \, I_L^{(3)}(\omega_0) + \dots \quad . \end{aligned} \tag{10.29}$$

Rearrangement of (10.29) yields, after applying some trigonometric relations,

$$\begin{aligned} I_L(\omega) = {} & I_L(\omega_0) + \frac{a^2}{4} I_L^{(2)}(\omega_0) + \frac{a^4}{64} I_L^{(4)}(\omega_0) + \dots \\ & + \left[a \, I_L^{(1)}(\omega_0) + \frac{a^3}{8} I_L^{(3)}(\omega_0) + \dots\right] \sin\Omega t \\ & + \left[-\frac{a^2}{4} I_L^{(2)}(\omega_0) - \frac{a^4}{48} I_L^{(4)}(\omega_0) + \dots\right] \cos 2\Omega t \\ & + \left[-\frac{a^3}{24} I_L^{(3)}(\omega_0) - \frac{a^5}{384} I_L^{(5)}(\omega_0) + \dots\right] \sin 3\Omega t \\ & + \dots \quad . \end{aligned} \tag{10.30}$$

The expressions in brackets yield the laser intensity at the nth harmonic of the modulation frequency Ω. The signal at 3Ω is therefore essentially determined by the third derivative $I_L^{(3)}(\omega_0)$ since at a sufficiently small modulation amplitude a, the second terms in the brackets are small compared to the first ones.

Figure 10.28 shows the experimental performance. The modulation frequency Ω is tripled by forming rectangular pulses, where the third harmonic is filtered and is fed into the reference input of a lock-in amplifier, which is tuned to 3Ω. The lock-in output is used for the stabilization feedback. Figure 10.29 illustrates a third derivative spectrum of the hyperfine structure components of I_2, obtained in Fig.10.23 with the intermodulated fluorescence technique.

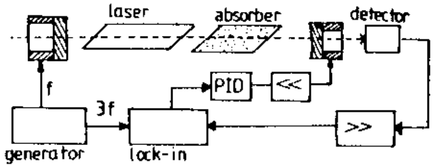

▲ Fig.10.28. Schematic arrangement for third derivative frequency stabilization

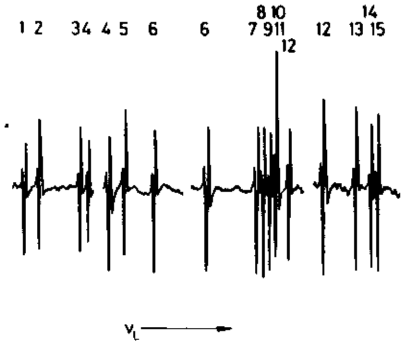

◄ Fig.10.29. Third derivative intracavity absorption spectrum of I_2 around $\lambda = 514.5$ nm, showing the same hfs components as Fig.10.23 [10.37a]

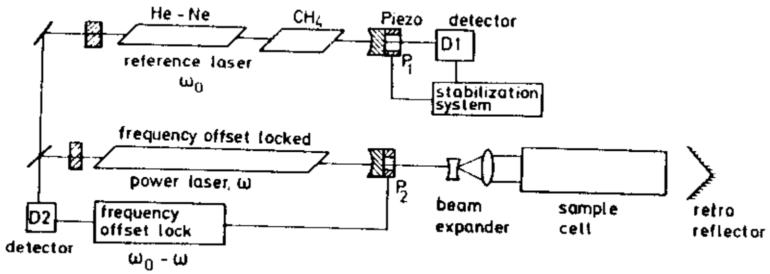

Fig.10.30. Schematic diagram of a frequency offset-locked spectrometer

Lamb dip stabilization onto very narrow saturation peaks allows one to achieve a very good frequency stability, especially when pressure or power broadening or transit broadening can be minimized, as in the case of the 3.39 μm He-Ne laser stabilized onto a CH_4 transition.

Using a double servo loop for fast stabilization of the laser frequency onto the transmission peak of a Fabry-Perot interferometer and a slow loop to stabilize the F.P.I. onto the first derivative of a forbidden narrow calcium transition BARGER et al. [10.44] constructed an ultrastable cw dye laser with a short-term linewidth of approximately 800 Hz and a long-term drift of less than 2 kHz/hr [10.45].

This extremely high stability can be transferred to tunable lasers by a special "frequency offset locking" technique [10.43] (see also Sect.6.9). Its basic principle is illustrated in Fig.10.30. A reference laser is frequency stabilized onto the Lamb dip of a molecular transition. The output from a second, more powerful laser at frequency ω is mixed in detector D 2 with the output from the reference laser at frequency ω_0. An electronic device compares the difference frequency $\omega_0 - \omega$ with the frequency ω' of a stable but tunable rf oscillator, and controls the piezo P_2 such that always $\omega_0 - \omega = \omega'$. The frequency ω of the power laser is therefore always locked to the "offset frequency" $\omega_0 - \omega'$ which can be controlled by tuning the rf frequency ω'.

The output beam of the power laser is expanded before it is sent through the sample cell in order to minimize transit time broadening (see Sect.3.4). A retroreflector provides the counter propagating probe wave for Lamb dip spectroscopy.

The spectrum in Fig.10.26 has been obtained with such a frequency offset locked laser spectrometer. The real experimental setup is somewhat more complicated. A third laser is used to eliminate the troublesome region near zero offset frequency. Furthermore optical decoupling elements have to be inserted to avoid optical feedback between the three lasers. A detailed description of the whole system can be found in [10.38].

10.2.4 Saturation Spectroscopy of Coupled Transitions

Assume that two laser fields are interacting simultaneously with a molecular system. If the two laser frequencies ω_1 and ω_2 are tuned to two molecular transitions which share a common level (a), coupling phenomena occur due to the nonlinear interaction between the fields and the molecular system. The absorption of one of the laser waves is influenced by the presence of the other wave. This coupling is caused by several different effects.

The first coupling effect is due to the selective saturation of the level population by each wave. When, for example, the frequency ω_1 is tuned close to the molecular transition a → b with $\omega_{ab} = (E_b - E_a)/\hbar$, the wave can be absorbed by molecules with velocity components $v_z \pm \Delta v_z = (\omega_{ab} - \omega_1 \pm \delta\omega)/k_1$. This causes a Bennet hole in the population distribution $n_a(v_z)$ (see Fig. 10.17). When the second laser is tuned over the absorption profile of the transition a → c, the Bennet hole causes a decrease in absorption of this laser. This can be monitored for instance by the corresponding decrease of the fluorescence intensity on the transition c → m (Fig.10.31).

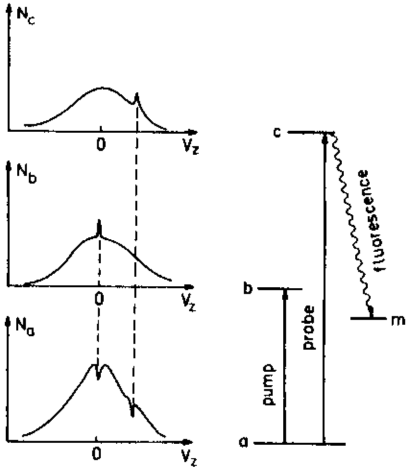

Fig.10.31. Coupling of two transitions a→ b and a→ c by saturation of the common level (a)

This optical-optical double resonance has been already discussed in Sect.8.9 as a method of labelling molecular levels and identifying molecular transitions in complex spectra. There we had not, however, considered the line profiles of the double resonance limits, which will be the subject of this section.

Since the two transitions are coupled only by those molecules within the velocity range Δv_z which have been pumped by one of the lasers, the double-resonance signals show similarly small homogeneous linewidths as in saturation spectroscopy with a single laser. However, for precise spectroscopy the common Bennet hole should be *exactly at the center* of the population distribution and not anywhere around $v_z = 0$. This can be achieved for instance by using the Lamb dip, produced in the *standing wave* of the pump field, to stabilize the pump laser frequency ω to the center frequency ω_{ab}.

The general case can be described as follows.

The absorption coefficient for the weak probe wave with frequency ω_2 is, according to (10.21),

$$\alpha(\omega_2) = \int [n_a(v_z) - n_c(v_z)] \frac{\sigma_0 \gamma_{ac}^2}{4(\omega_{ac} - \omega_2 - k_2 v_z)^2 + \gamma_{ac}^2}\, dv_z \quad . \qquad (10.31)$$

The population density $n_a(v)$ is altered by the saturating pump transition a → b. With a pump laser frequency ω_1 we obtain, according to (10.20),

$$n_a(v_z) - n_c(v_z) = n_a^0(v_z) - n_c^0(v_z) - \frac{[n_a^0(v_z) - n_b^0(v_z)](\gamma_{ab}/2)^2 S}{(\omega_{ab} - \omega_1 - k_1 v_z)^2 + (\gamma_{ab}/2)^2} \qquad (10.32)$$

where the saturation parameter $S = B_{ab}\rho(\omega_1)/\gamma_{ab}$ depends on the intensity of the pump wave and γ_{ab} is the homogeneous width of transition a → b.

Inserting (10.32) into (10.31) yields the absorption coefficient $\alpha(\omega_2)$ of the probe wave in the presence of the saturating pump wave at frequency ω_1

$$\alpha(\omega_2) = \alpha_0 \exp -[(\ln 2)(\omega_{ac} - \omega_2)^2/\Delta\omega_D^2] \qquad (10.33)$$
$$\times \left\{1 - \frac{N_a^0 - N_b^0}{N_a^0 - N_c^0}\,\frac{k_2}{2k_1}\,\frac{S}{\sqrt{1+S}}\,\frac{\gamma^*}{[(\omega_{ac} - \omega_2) \pm (k_2/k_1)(\omega_{ab} - \omega_1)]^2 + \gamma^{*2}}\right\}$$

where $\gamma^* = \gamma_{ac} + (k_2/k_1)\gamma_{ab}\sqrt{1+S}$ and $N = \int n(v_z)dv_z$.

The + or - signs describe the cases where both waves travel in opposite directions, or in the same direction.

21

If the pump wave is stabilized to the line center ω_{ab}, the second term in the denominator vanishes, since $\omega_1 - \omega_{ab} = 0$ and the line contour of the saturation dip in the absorption profile $\alpha(\omega_2)$ is described by a Lorentzian-shaped profile

$$L^*(\omega) = \frac{\gamma^*}{(\omega_{ac} - \omega_2)^2 + \gamma^{*2}}$$

with a linewidth which is the sum of the homogeneous width γ_{ac} and the saturated Lamb dip width $(k_2/k_1)\gamma_{ab}\sqrt{1+S}$ of the pump wave times the ratio of the two laser frequencies ω_1 and ω_2.

One of many examples for the application of this optical-optical double-resonance technique is the precise determination of the CH_3F dipole moment values both for the ground and excited vibrational states [10.46]. The beams from two independent CO_2 lasers propagate collinearly through the sample in an electric field. Both lasers oscillate on the same CO_2 transitions, and their frequency difference $\omega_1 - \omega_2$ is set within the range 0-50 MHz by piezoelectric tuning of the optical cavity lenghts. Measurements of the beat frequency indicate a 20-30 KHz acoustic jitter over a 1 s interval. If the beat frequency is kept fixed but the voltage for the electric field in the sample is swept, the Stark splittings can be tuned into resonance with the beat frequency.

The two monochromatic laser waves can also be provided by two simultaneously oscillating modes of a multimode laser. If the absorbing sample is placed inside the laser resonator in a magnetic field, the molecular levels are split into the (2J + 1) Zeeman sublevels with a separation

$$\Delta\omega_z = \mu_B g B/\hbar \quad ,$$

where μ_B is the Bohr magneton, g the Landé factor, and B the magnetic field strength. If the Zeeman splitting $\Delta\omega_z$ equals the mode separation $\Delta\nu = c/2d$ of the laser resonator, two laser modes share a common level (see Fig.10.32).

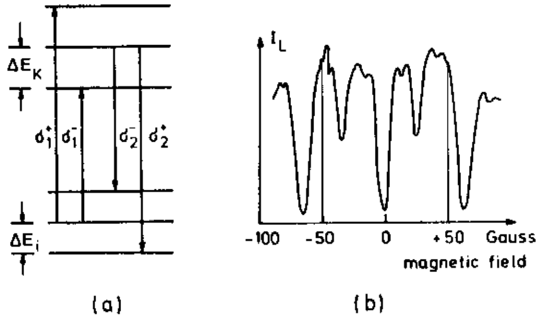

Fig.10.32a,b. Three-level laser spectroscopy with a multimode laser and Zeeman scanning. (a) Level scheme, (b) resonances in the laser output as a function of the magnetic field [10.47]

If both transitions share a common *lower* level, the absorption *decreases* for the resonance case due to the saturation of the lower level by both modes. The laser intensity therefore *increases*. If the two transitions share a common *upper* level, the laser output *decreases* at resonance, because the population of the *upper* level decreases, which diminishes the gain. This allows one to distinguish between the Zeeman splittings in the upper or the lower level and the Landé factors of both levels can be accurately measured [10.47,48].

An experimental advantage of this method is the fact that only the *difference* frequency between two modes and not the absolute frequency is essential for the spectral resolution. Such experiments can therefore be performed with unstabilized lasers.

Examples of two coupled transitions which have been thoroughly studied by several groups [10.49-51] are given by the two neon transitions at $\lambda = 0.63\ \mu m$ and $\lambda = 1.15\ \mu m$ which share the $^2P_4$ state as a common lower level, or the 0.63 μm and the 3.39 μm lines which share a common upper level (see Fig.6.7). Both coupled transitions show inversion in a He-Ne discharge and laser oscillation can be simultaneously achieved on both lines. The interaction of the two transitions can therefore be studied in a resonator arrangement which allows one to detect both laser lines separately. Figure 10.33 shows the concept and experimental arrangement. A single mode of the

He-Ne laser oscillating at $\lambda = 0.63\ \mu m$ is selected by a Fox-Smith cavity (see Sect.6.5) with a frequency ω_1 which can be continuously tuned through the gain profile of the laser transition. The output from a 1.15 μm He-Ne laser is sent collinear with the 0.63 μm beam through the gas discharge and is separated from the 0.63 μm by a prism. The attenuation or amplification of the 1.15 μm beam is detected as a function of the laser frequency ω_1 and of the inversion $n(3S_2) - n(2P_4)$, which can be altered by controlling the discharge conditions. The authors call this spectroscopic technique "tuned differential sepctroscopy".

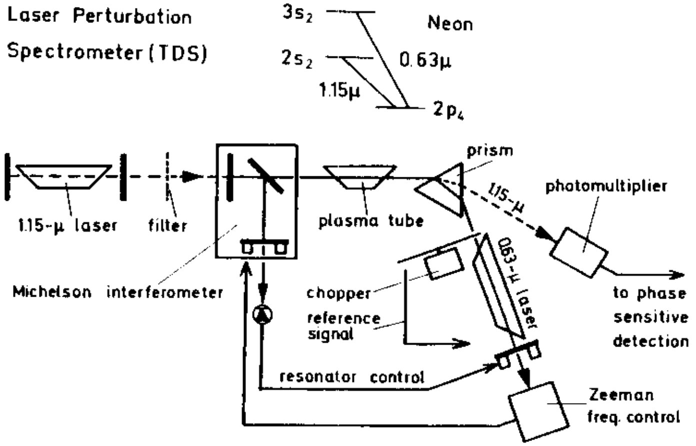

Fig.10.33. Optical-optical double resonance of two coupled Ne laser transitions studied in a tuned differential laser spectrometer [10.50]

The detailed studies show that the saturation of the common level, as discussed above, is not the only coupling mechanism. The interaction of the atom with a light wave generates an induced dipole moment which is at small intensities proportional to the field amplitude. At higher intensities the nonlinear terms in the induced polarization become important. If two waves with frequencies ω_1 and ω_2 simultaneously act in resonance with the atom, these nonlinear terms produce sum and difference frequencies $\omega_1 \pm \omega_2$. For two transitions which share a common level the difference frequency $\omega_1 - \omega_2$ is in resonance with the atomic transition $b \leftrightarrow c$ $(2S_2 - 3S_2)$ and will therefore modulate the atomic polarization at the frequency $\omega_1 - \omega_2$. The phenomenon can be regarded as a *resonant Raman process* where the 0.63 μm transition generates the Stokes line at $\lambda = 1.15\ \mu m$ and both waves force the electronic polarization to oscillate at the difference frequency (see Sect.9.4).

The study of these parametric interactions allows one to gain detailed information on the nonlinear polarization of the atom, and on the energy shift of the participating levels under the influence of the two fields for resonance and off-resonance conditions. The interaction is different for the two cases where the waves at 1.15 and 0.63 nm propagate in the same or opposite directions [10.52], see (10.33).

This section on saturation spectroscopy could only give a brief survey on this field and tried to illustrate the method by a few examples. A much more detailed discussion with more examples and extensive references can be found in [10.53-55].

10.3 Polarization Spectroscopy

While saturation spectroscopy monitors the decrease of *absorption* of a probe beam caused by a pump wave which has selectively depleted the absorbing level, the signals in polarization spectroscopy come mainly from the change of *refractive index* induced by a polarized pump wave [10.56]. This very sensitive Doppler-free spectroscopic technique has many advantages over conventional saturation spectroscopy and will certainly gain increasing attention [10.56a-c]. We therefore discuss the basic principle and some of its experimental modifications in more detail.

10.3.1 Basic Principle

The basic idea of polarization spectroscopy can be understood in a simple way (Fig.10.34).

The output from a monochromatic tunable laser is split into a weak probe beam with intensity I_1 and a stronger pump beam with intensity I_2. The probe beam passes through a linear polarizer P_1, the sample cell, and a second linear polarizer P_2 which is nearly crossed with P_1. At a crossing angle $(\pi/2 - \theta)$ with $\theta \ll 1$, only the component $E_t = E_0 \sin\theta \approx E_0\theta$ can pass through P_2 and reaches the detector D.

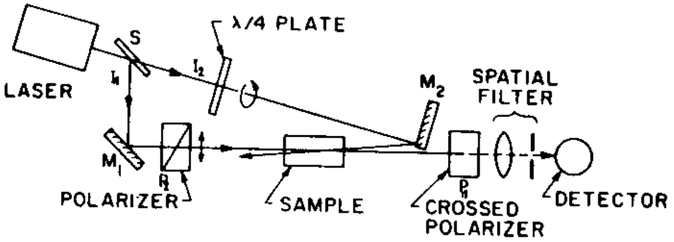

Fig.10.34. Schematic experimental arrangement for polarization spectroscopy [10.57]

After having passed a λ/4 plate which produces a circular polarization, the pump beam travels *in the opposite direction* through the sample cell. When the laser frequency ω is tuned to a molecular transition $(J'', M'') \to (J',M')$, molecules in the lower level (J'', M'') can absorb the pump wave. The quantum number M, which describes the projection of J onto the direction of light propagation, follows the selection rule $\Delta M = +1$ for transitions $M'' \to M'$ induced by left-hand circularly polarized light $(M'' \to M' = M'' + 1)$. Due to saturation the degenerate M sublevels of the rotational level J" become partially or completely depleted. The degree of depletion depends on the pump intensity I_2, the absorption cross section $\sigma(J'', M'' \to J', M')$, and on possible relaxation processes which may repopulate the level (J'', M''). The cross section σ depends on J", M", J', and M'. From Fig.10.35 it can be seen that in case of P or R transitions ($\Delta J = +1$ or -1), not all of the M sublevels are pumped. For example from levels with $M'' = +1,+2$, no P transitions with $\Delta M = +1$ are possible while for R-transitions the levels $M' = -1,-2$, are not populated. This implies that *the pumping process produces an unequal saturation and with it a nonuniform population of the M sublevels*, which is equivalent to an anisotropic distribution for the orientations of the angular momentum vector J.

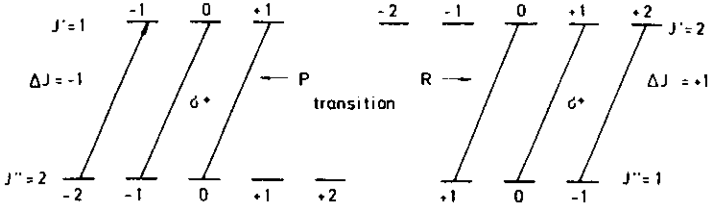

Fig.10.35. Selective depopulation of different M" sublevels and selective population of different M' sublevels by optical pumping with circularly polarized σ^+ light

Such an anisotropic sample becomes birefringent for the incident linearly polarized probe beam, and the plane of polarization is slightly rotated. This effect is quite analogous to the Faraday effect where the nonisotropic orientiation of J is caused by an external magnetic field. For polarization spectroscopy no magnetic field is needed. Contrary to the Faraday effect where all molecules are oriented, here only those molecules which interact with the monochromatic pump wave show this nonisotropic orientation. As has already been discussed in Sect.10.1, this is the subgroup of molecules with velocity components

$$v_z \pm \Delta v_z = (\omega_0 - \omega)/k \pm \delta\omega/k \quad ,$$

where Δv_z is determined by the homogeneous linewidth $\delta\omega = \gamma$.

For $\omega \neq \omega_0$ the probe wave which passes in the opposite direction through the sample interacts with a *different* group of molecules in the velocity interval $v_z \pm \Delta v_z = -(\omega_0 - \omega \pm \delta\omega)/k$, and will therefore not be influenced by the pump wave. If, however, the laser frequency ω coincides with the center frequency ω_0 of the molecular transition within its homogeneous linewidth $\delta\omega$ (i.e., $\omega = \omega_0 \pm \delta\omega \Rightarrow v_z = 0 \pm \Delta v_z$), both waves can be absorbed by the same molecules and the probe wave experiences a birefringence due to the nonisotropic M distribution of the absorbing molecules.

Only in this case will the plane of polarization of the probe wave be slightly rotated by $\Delta\theta$ and the detector D will receive a Doppler-free signal every time the laser frequency ω is tuned across the center of a molecular absorption line.

10.3.2 Line Profiles of Polarization Signals

Let us now discuss the generation of this signal in a more quantitative way following the presentation in [10.57]. The linearly polarized probe wave

$$\underline{E} = \underline{E}_0\, e^{i(\omega t - kz)} \quad , \quad \underline{E}_0 = \{E_{0x}\ ,\ 0\ ,\ 0\}$$

can be always composed of a right and a left circularly polarized component (Fig.10.36). While passing through the sample the two components experience different absorption coefficients α^+ and α^- and different refractive indices n^+ and n^- due to the nonisotropic saturation caused by the left circularly polarized pump wave. After a path length L through the pumped region of the sample the two components are

$$E^+ = E_0^+\, e^{i[\omega t - k^+L + i(\alpha^+/2)L]} \quad ; \quad 2E_0^+ = E_{0x} + iE_{0y}$$

$$E^- = E_0^-\, e^{i[\omega t - k^-L + i(\alpha^-/2)L]} \quad ; \quad 2E_0^- = E_{0x} - iE_{0y} \quad . \tag{10.34}$$

Due to the differences $\Delta n = n^+ - n^-$ and $\Delta\alpha = \alpha^+ - \alpha^-$ caused by the nonisotropic saturation, a phase difference

$$\Delta\varphi = (k^+ - k^-)L = (\omega L/c)(n^+ - n^-)$$

has developed between the two components and also a small amplitude difference

$$\Delta E = (E_0/2)\left[e^{-(\alpha^+/2)L} - e^{-(\alpha^-/2)L}\right] \ .$$

If both components are again superimposed at $z = L$ after having passed through the sample cell, an elliptically polarized wave comes out with a major axis which is slightly rotated against the x axis. The y component of this elliptical wave is

$$E_y = -i(E_0/2)\, e^{i[k^+ - k^- + i(\alpha^+ - \alpha^-)/2]L + ib}\, e^{i(\omega t + \varphi)} \quad , \tag{10.35}$$

where the term ib with $b \ll 1$ in the exponent takes into account that the windows of the sample cell may have a small birefringence which introduces an additional ellipticity. In all practical cases the differences $\Delta\alpha$ and Δk are small,

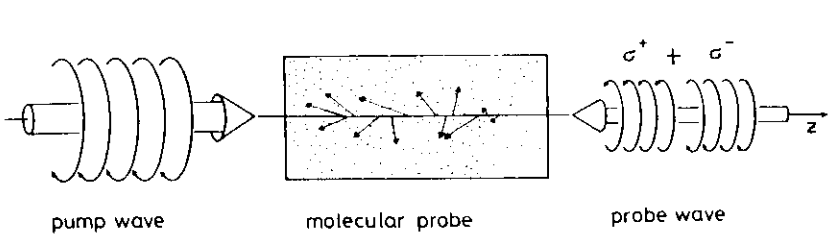

Fig.10.36. Schematic illustration of partial alignment of angular momenta by the left-hand circularly polarized (σ^+) pump wave, which results in different absorption coefficients for σ^+ and σ^- probe light

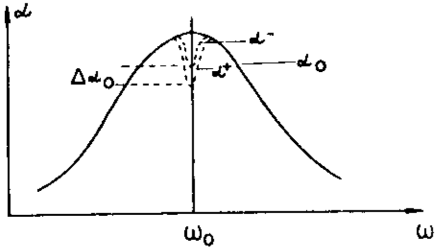

Fig.10.37. Spectral profiles of the absorption coefficients α^+ and α^- for a weak probe, in the presence of a saturating counterpropagating pump

$$(\alpha^+ - \alpha^-)L \ll 1 \quad \text{and} \quad (k^+ - k^-)L \ll 1 \quad ,$$

and we can expand the first exponential factor. If the transmission axis of the second polarizer P_2 is close to the y axis ($\theta \ll 1$), we obtain for the transmitted amplitude

$$E_t = E_0[\theta + ib + (\omega L/2c)(n^+ - n^-) + i(\alpha^+ - \alpha^-)L/4]e^{i(\omega t + \varphi)} \quad . \tag{10.36}$$

The differences $\Delta\alpha = \alpha^+ - \alpha^-$ in absorption coefficients and $\Delta n = n^+ - n^-$ in refractive indices are due to the different degrees of M sublevel depopulations experienced by the right or the left circularly polarized probe component. Although each coefficient α^+ and α^- itself shows a Doppler-broadened spectral profile with a Lamb dip at the center, the *difference* $\Delta\alpha$ just exhibits the small difference between these Lamb dips (see Fig.10.37) The spectral profile of $\Delta\alpha$ is therefore Lorentzian

$$\Delta\alpha = \frac{\Delta\alpha_0}{1 + x^2} \quad \text{with} \quad x = (\omega_0 - \omega)/\gamma \quad , \tag{10.37}$$

where $\Delta\alpha_0$ is the maximum difference at the center $\omega = \omega_0$. Since absorption and dispersion are related by the *Kramers-Kronig dispersion relations* (see Sect.2.6), we obtain a dispersion shaped profile for Δn

$$\Delta n = \Delta\alpha_0 \frac{c}{\omega_0} \frac{x}{1 + x^2} \quad . \tag{10.38}$$

The transmitted intensity is $I_T = E_T E_T^*$. Taking into account that even perfectly crossed polarizers show a residual transmission $I_0\xi$ with $\xi \ll 1$ due to imperfect extinction, we obtain the spectral line profile of the transmitted intensity I_T from (10.35-38).

$$I_T = I_0\left[\xi + \theta^2 + b^2 - \frac{1}{2}\,\theta\Delta\alpha_0 L \frac{x}{1 + x^2} + \frac{b}{2}\,\Delta\alpha_0\,L \frac{1}{1 + x^2} + \frac{1}{4}\,(\Delta\alpha_0 L)^2 \frac{1}{1 + x^2}\right] \quad . \tag{10.39}$$

The transmitted intensity contains a constant background term $\xi + \theta^2 + b^2$ which is caused: 1) by the finite transmission $I_0\xi$ of the crossed polarizers at $\theta = 0$; 2) by the birefringence of the cell windows, described by the term $I_0 b^2$ and 3) by the finite uncrossing angle θ of P_2. The birefringence of the windows can be controlled, for example, by squeezing the windows slightly to compensate for the birefringence which is mainly caused by the pressure difference of 1 atm at both sides of the windows. A proper selection of the uncrossing angle θ and the window birefringence b allows one to make either the first Lorentzian term dominant ($\theta = 0$, b large) or the dispersion term ($\theta \neq 0$, b small). If for the latter choice $\theta \gg \Delta\alpha_0 \cdot L$, the last Lorentzian term becomes negligible and one obtains nearly pure dispersion profiles, while for the former choice pure Lorentzian profiles are monitored.

Figure (10.38) shows an example of a section from the polarization spectrum of the cesium molecule Cs_2, recorded with $\theta = 0$ (lower part) and with $\theta = 2.5' \hat{=} \theta = 7 \times 10^{-4}$ rad (upper part). In this experiment the term $(\xi + b^2)$ was smaller than 10^{-6}.

Note that the main contribution to the signal comes from the *rotation* of the plane of polarization of the linearly polarized probe wave, and only to a minor extent from the change of absorption $\Delta\alpha$. In (10.39) $\Delta\alpha$ appears because $\Delta n = n^+ - n^-$ has been replaced by $\Delta\alpha$ using the dispersion relations. It is the difference in *phase shifts* for the two probe components E^+ and E' rather than the slightly different amplitudes which gives the major part of the signal. The reason why this method is much more sensitive than the saturation method, is due to the crossed polarizers which suppress the background.

A linearly, rather than circularly, polarized pump wave can also be used with the plane of polarization inclined by 45° against that of the probe. Assume that the pump wave is polarized in the x direction. The probe wave then

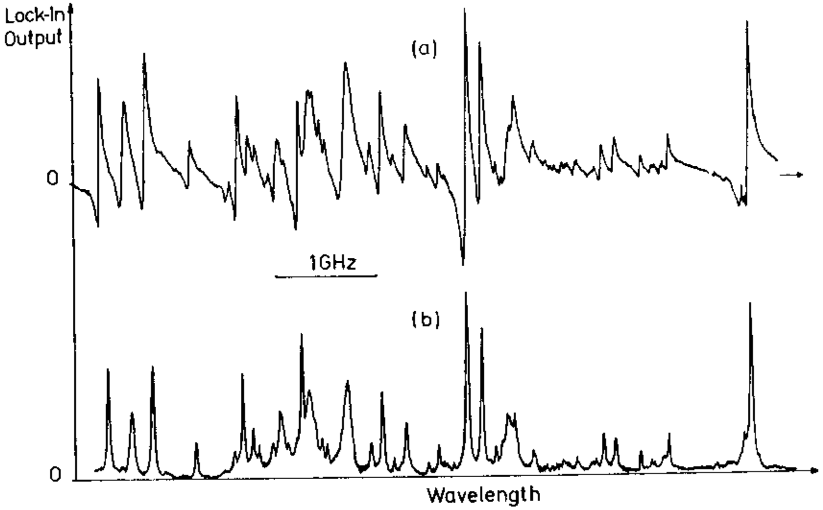

(a) Cs_2, $\lambda = 488$ nm, ↻Pump, $\theta = 3'$; (b) Cs_2, $\lambda = 488$ nm, ↻Pump, $\theta = 0'$;

Fig.10.38a,b. Two identical sections of Cs_2 polarization spectra obtained with circular pump polarization and linear probe polarization, but different uncrossing angles θ of the two polarizers [10.59]

can be composed of two linearly polarized components E_x and E_y and the saturation by the pump will cause a difference $\alpha_x - \alpha_y$ and $n_x - n_y$. Analogous to the derivation above we obtain in this case for the probe intensity, transmitted through the polarizer P_2,

$$I_T = I_0\left[\xi + \theta^2 + b^2 + \frac{1}{2}\,\theta\Delta\alpha L \frac{1}{1 + x^2} + \frac{1}{2}\,b\Delta\alpha L \frac{x}{1 + x^2} + \frac{1}{4}\,(\Delta\alpha L)^2 \frac{1}{1 + x^2}\right] \quad , \tag{10.40}$$

which shows that the dispersion term and the Lorentzian term are just interchanged compared to (10.39). For b = 0 (no birefringence of the cell windows) and $\theta \neq 0$ (polarizers not completely crossed) we obtain pure Lorentzian profiles.

10.3.3 Magnitude of Polarization Signals

In order to estimate the expected magnitudes of the polarization signals in (10.39) let us consider the difference $\Delta\alpha = \alpha^+ - \alpha^-$ in the absorption coefficients for the right- and left-hand circularly polarized probe wave components. The absorption of a circularly polarized wave tuned to a rotational transition $J \rightarrow J_1$ is due to the sum of all allowed transitions $M_J \rightarrow M_{J_1}$ with $\Delta M = \pm 1$ between the $(2J + 1)$ degenerate sublevels M in the lower level J and the $(2J_1 + 1)$ sublevels in the upper level J_1.

$$\alpha^+ - \alpha^- = \sum_M n_M(\sigma^+_{JJ_1M} - \sigma^-_{JJ_1M}) \quad , \tag{10.41}$$

where $\sigma^\pm_{JJ_1M}$ is the absorption cross section for the transition $(J, M) \rightarrow (J_1, M+1)$ or $(J, M) \rightarrow (J_1, M-1)$.

The M dependence of the cross sections σ_{JJ_1M} can be expressed in terms of Clebsch-Gordan coefficients $C(J, J_1, M, M_1)$ and a reduced matrix element $\tilde{\sigma}_{JJ_1}$ which is independent of M and describes the total rotational transition $J \rightarrow J_1$ [10.58]. The explicit evaluation yields for a circularly polarized pump wave

$$\sigma^\pm_{JJ_1M} = \begin{cases} \tilde{\sigma}_{J,J+1}(J \pm M + 1)\,(J \pm M + 2) & \text{for} \quad J_1 = J + 1 \\ \tilde{\sigma}_{J,J}(J \pm M)\,(J \pm M + 1) & \text{for} \quad J_1 = J \\ \sigma_{J,J-1}(J \mp M)\,(J \pm M + 1) & \text{for} \quad J_1 = J - 1 \quad . \end{cases} \tag{10.42}$$

For a linearly polarized pump wave the analogous calculation yields

$$\sigma_{JJ_1M} = \begin{cases} \tilde{\sigma}_{J,J+1}(J + 1)^2 - M^2 & \text{for R lines} \\ \tilde{\sigma}_{J,J}\, M^2 & \text{for Q lines} \\ \tilde{\sigma}_{J,J-1}(J^2 - M^2) & \text{for P lines} \quad . \end{cases} \tag{10.42a}$$

The total cross section

$$\sigma_{JJ_1} = \frac{1}{2J + 1} \sum_M \sigma_{J,J_1M}$$

for the transition $J \rightarrow J_1$ is independent of the kind of polarization. Inserting (10.42) and evaluating the sum over M yields

$$\sigma_{JJ_1} = \frac{1}{3}\,\tilde{\sigma}_{JJ_1} \begin{cases} (J + 1)(2J + 3) & \Delta J = +1 \\ J(J + 1) \quad \text{for} & \Delta J = 0 \\ J(2J - 1) & \Delta J = -1 \quad . \end{cases} \tag{10.43}$$

The unsaturated level population of a sublevel M is

$$n^0_M = N_0/(2J + 1) \quad . \tag{10.44}$$

where N_0 is the unsaturated total population of the rotational level J. Without the saturating pump wave, we obtain by inserting (10.43) and (10.44) into (10.41)

$$\Delta\alpha^0 = \alpha^+ - \alpha^- = 0 \quad .$$

Due to saturation by the pump wave with intensity I_2 the population of the M sublevels decreases according to (2.167) to

$$n^{(s)}_M = \frac{N_0}{2J + 1} \cdot \frac{1}{1 + S_M} \tag{10.44a}$$

and the absorption of the probe wave by molecules in sublevel M decreases according to (10.23) to

$$\alpha^s_M = \alpha^0_M(1 - S_M) \quad .$$

The saturation parameter S_M at the line center ω_0 [see (2.73) and (3.70)],

$$S_{0M} = 2S_M/(\pi\gamma_s) = \frac{8I_2\sigma_{JJ_1M}}{c\gamma_s R\hbar\omega} \quad , \tag{10.45}$$

depends on the absorption cross section σ_{JJ_1M} of the pump wave, on the number $n_p = I_2/\hbar\omega$ of pump photons incident on the sample per cm^2 and s, on the saturation-broadened homogeneous linewidth γ_s, and on the collision induced relaxation rate R [s^{-1}] which tries to refill the depleted level and depopulate the upper level. In Fig.10.39 the M dependence of σ_{JJ_1M} is plotted for right-hand and left-hand circular polarization and for linear polarization (second column). These diagrams illustrate that saturation by a *circularly* polarized pump wave results in larger differences $(\alpha^+ - \alpha^-)$ for P and R lines than for Q lines, while a linearly polarized pump wave favors Q lines in the detected probe transmission.

Putting the relations (10.41-45) together, we can express the difference $\alpha^+ - \alpha^-$ at the line center ω_0 by the unsaturated absorption coefficient $\alpha_0 = N^0_J\sigma_{JJ_1}$, the saturation parameter $S_0(\omega_0)$, and a numerical factor $C^*_{JJ_1}$ which stands for the sum over the Clebsch-Gordan coefficients and which is tabulated in [10.57]. The final result is

$$\alpha^+ - \alpha^- = \alpha^0 S_0 C^*_{JJ_1} \quad . \tag{10.46a}$$

This is often written in the form

$$\boxed{\alpha^+ - \alpha^- = \alpha^0 C^*_{JJ_1}\,(I_2/I_S)} \quad , \tag{10.46b}$$

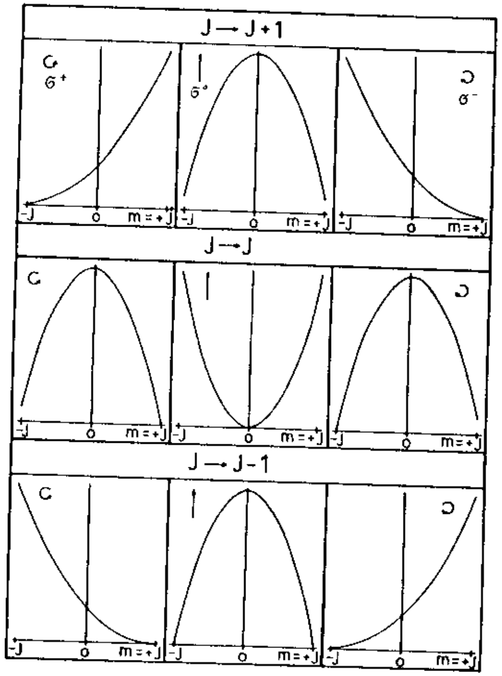

Fig.10.39. M dependence of the cross section σ_{JJ_1M} for P, Q, and R lines for σ^+, σ^-, and $\sigma^0 = \pi$-polarized light

where $I_S = I_2/S_0$ represents that pump intensity which causes a saturation parameter $S_0 = 1$ at the line center.

10.3.4 Sensitivity of Polarization Spectroscopy

In the following we briefly discuss the sensitivity and the signal-to-noise ratio achievable with polarization spectroscopy. The amplitude of the dispersion signal in (10.39) is approximately the difference $\Delta I_T = I_T(x = +1) - I_T(x = -1)$ between the maximum and the mimimum of the dispersion curve. From (10.39) we obtain

$$\Delta I_T = \frac{1}{2}\,\theta\Delta\alpha L \quad . \tag{10.47}$$

Under general laboratory conditions the main contribution to the noise comes from fluctuations of the probe laser intensity, while the principal limit set by shot noise (see Chap.4) is seldom reached. The noise level is therefore essentially proportional to the transmitted intensity, which is given by the background term in (10.39).

Because the crossed polarizers greatly reduce the background level, we can expect a better signal-to-noise ratio than in saturation spectroscopy, where the full intensity of the probe beam is detected.

In the absence of window birefringence (i.e., b = 0) the signal-to-noise ratio (S/N) which is, besides a constant factor a, equal to the signal-to-background ratio, becomes

$$S/N = \frac{\theta\alpha_0 L(I_p/I_s)}{a(\xi + \theta^2)}\, C^*_{JJ_1} \quad . \tag{10.48}$$

This ratio has a maximum for $d(S/N)/d\theta = 0$ which yields

$$(S/N)_{\max} = \frac{\alpha_0 L(I_p/I_s)}{a\xi^{1/2}}\, C^*_{JJ_1} \tag{10.49}$$

for $\theta^2 = \xi$.

According to (10.23) the signal-to-background ratio is for saturation spectroscopy outside the laser resonator

$$(S/N)_{\mathrm{sat}} = \alpha_0 I L S_0/I = \alpha_0 L I_p/I_s \quad ,$$

while a value of I_p/I_s may be reached with the intermodulated fluorescence technique [10.33]. Equation (10.49) shows that a factor of $\xi^{-1/2}$ is gained in polarization spectroscopy. Since good polarizers allow an extinction ratio of $\xi = 10^{-6} - 10^{-7}$, the enhancement of the signal-to-background ratio may become three orders of magnitude. Only for $\alpha_0 L < 10^{-3}$ can the intermodulated fluorescence method compete with polarization spectroscopy. The sensitivity of polarization spectroscopy is demonstrated by Fig.10.40 which shows a section of the polarization spectrum of NO_2 where the three hfs components of each transition are resolved. The transition probabilities of NO_2 transitions are very small. This impedes saturation spectroscopy but still allows polarization spectroscopy because of its higher sensitivity.

With a circularly polarized pump wave the P and R lines show dispersion profiles (Fig.10.40a) while for a linearly polarized pump wave the Q lines are monitored with Lorentzian profiles. Note that the whole range between the arrows in Fig.10.40a covers only 0.01 cm^{-1} = 0.0024 Å. The linewidth of about 5 MHz is limited mainly by the finite crossing angle between pump beam and probe beam. It can be further reduced by enlarging the length L of the sample cell.

For illustration of the achievable signal-to-noise ratio, Fig.10.41 shows the polarization spectrum of the same R(98) hfs components of I_2 as obtained

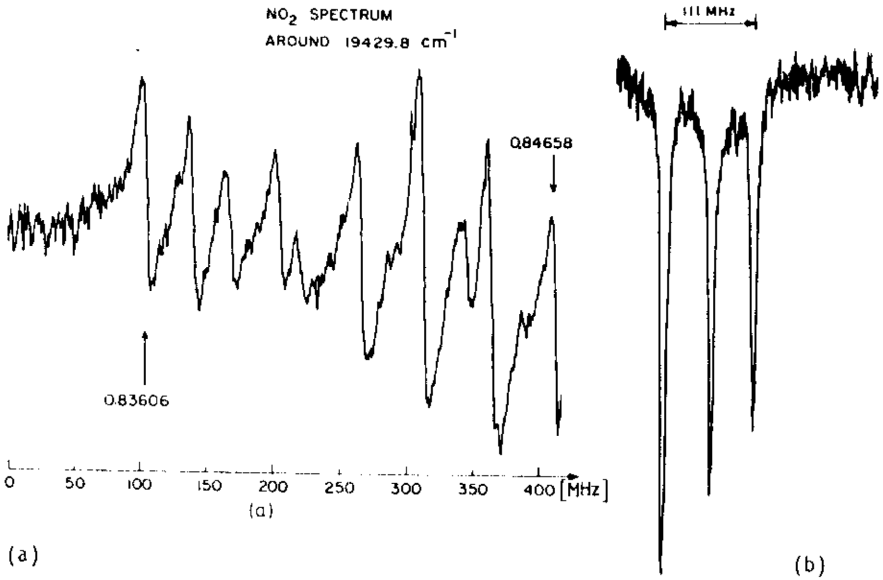

Fig.10.40a,b. Section of a polarization spectrum of NO_2 around λ = 488 nm. (a) Circular pump polarization, (b) linear pump polarization. The linewidth of 5 MHz is mainly determined by the residual Doppler width, due to the crossing angle between pump and probe beam

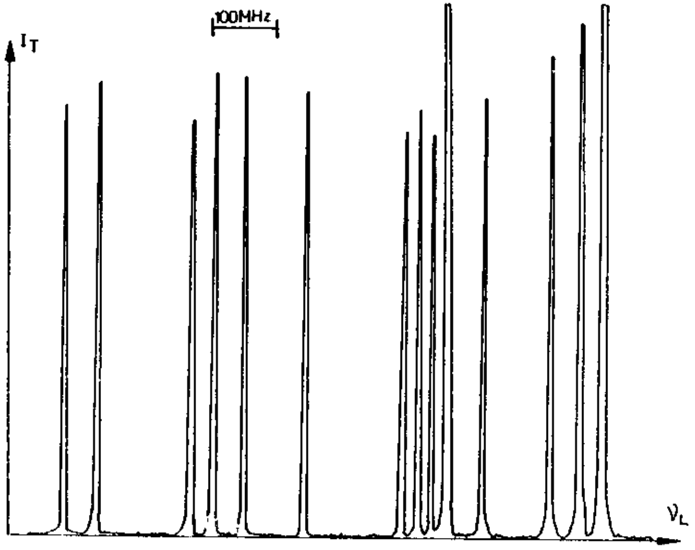

Fig.10.41. Polarization spectrum of the hfs components of the R(98), 58 - 1 line of I_2 at 514.5 nm (compare with Fig.10.23)

in Fig.10.23 with intermodulated fluorescence saturation spectroscopy. The polarization spectrum shows a signal-to-noise ratio which is better by two orders of magnitude.

10.3.5 Polarization Labelling Spectroscopy

A very powerful method for the assignment of complex molecular spectra is the "polarization labelling technique", which is based on a combination of polarization spectroscopy and optical double resonance. This method employs two different lasers (see Fig.10.42). The output beam from the first laser is again split into a pump beam and a probe beam and the laser frequency is stabilized onto the center frequency ω_0 of a polarization signal. The probe beam from the second laser passes collinearly with the probe beam from the first laser through the sample cell. Both beams are separated by a prism and are separately detected. When the frequency of the "probe laser" is tuned across the molecular absorption spectrum, a polarization signal is obtained every time the probe laser hits a transition which shares a common level with the pump transition (see Fig.8.36).

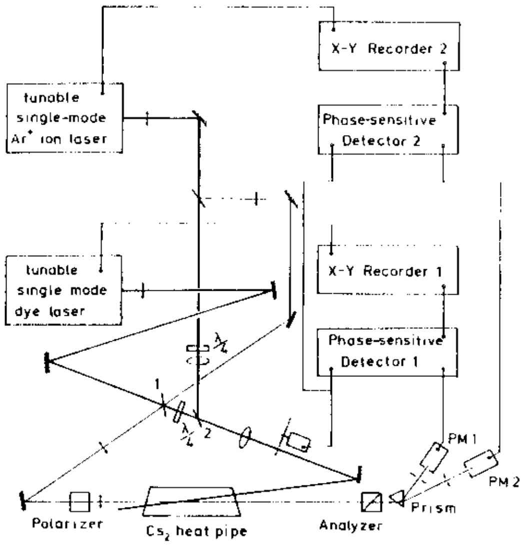

Fig.10.42. Experimental arrangement for polarization labelling spectroscopy

Evaluation of the cross sections (see [10.57]) shows that the form, sign, and magnitude of the signals depend on the kind of polarization of the pump wave and on the value of ΔJ_1 and ΔJ_2 for pump and probe transition. This gives

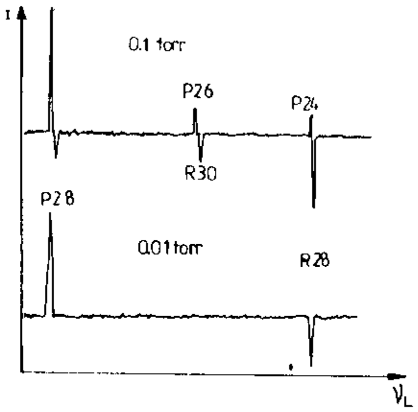

Fig.10.43. Optical-optical double-resonance lines in the polarization spectrum of Na_2. The pump laser was a single-mode argon laser, stabilized onto the transition $X^1\Sigma$ ($v''=0$, $J''=28$) → B^1($v'=6$, $J'=27$). The broad-band dye laser was scanned across the X → A-spectrum. At low pressures only the transitions ($v''=0$, $J''=28 \to J'=28\ \ 1$) appear as double resonance signals while at 0.1 torr collision-induced satellites are generated

the possibility of distinguishing even P lines from R lines in the double-resonance spectrum, because the two signals have opposite signs if the pump laser is stabilized on an R or P transition [10.59]. Figure 10.43 illustrates such a double-resonance spectrum of Na_2 where the opposite sign of P and R lines can be seen.

This technique is particularly useful if the upper state is perturbed and the assignment by conventional spectroscopy is impeded [10.61].

The second probe beam may be a broadband laser. If the polarization signal is detected on a photoplate behind a spectrograph, many transitions from the labelled level can then be detected simultaneously [10.61a].

The orientation of the molecules due to saturation by a polarized pump wave can be partly transferred to neighbouring levels by inelastic collisions of the oriented molecules with other atoms or molecules. This produces "satellite lines" in the double-resonance spectrum which may partly diminish the unambiguity of line assignment. Some of the weaker lines in Fig.10.43 are such collision-induced polarization signals.

10.3.6 Advantages of Polarization Spectroscopy

Let us briefly summarize the advantages of polarization spectroscopy, discussed in the previous sections.

1) With the other sub-Doppler techniques it shares the advantage of high spectral resolution which is mainly limited by the residual Doppler width due to the finite angle between pump beam and probe beam. This limitation corresponds to that imposed to linear spectroscopy in collimated molecular beams by the divergence angle of the molecular beam. The time-of-flight broadening can be reduced if pump and probe beam are less tightly focussed.

2) The sensitivity is 2-3 orders of magnitude larger than that of saturation spectroscopy. It is surpassed only at very low sample pressures by that of the intermodulated fluorescence technique (Sect.10.2.3).

3) The possibility of distinguishing between P, R, and Q lines is a particular advantage for the assignment of complex molecular spectra.

4) The dispersion profile of the polarization signals allows a stabilization of the laser frequency to the line center without any frequency modulation. The large achievable signal-to-noise ratio assures an excellent frequency stability.

5) The combination of optical-optical double resonance techniques and polarization spectroscopy opens the way to detailed studies of perturbed excited molecular states.

10.3.7 Doppler-Free Laser-Induced Dichroism and Birefringence

A slight modification of the experimental arrangement used for polarization spectroscopy allows the simultaneous observation of saturated absorption *and* dispersion [10.62]. While in the setup of Fig.10.34 the probe beam had linear polarization, here a circularly polarized probe and a linearly polarized pump beam are used (Fig.10.44). The probe beam can be composed of two components with linear polarization parallel and perpendicular to the pump beam polarization. Due to anisotropic saturation by the pump, the absorption coefficients $\alpha_\parallel$ and $\alpha_\perp$ and the refractive indices $n_\parallel$ and $n_\perp$ experienced by the probe beam are different for the parallel and the perpendicular polarizations. This causes a change of the probe beam polarization which is monitored behind a linear analyzer rotated through an angle β from the reference direction π. Analogous to the derivation in Sect.10.3.2, one can show that the transmitted intensity of a circularly polarized probe wave with incident intensity I is for $\alpha L \ll 1$ and $\Delta n(L/\lambda) \ll 1$

$$I_t(\beta) \approx \frac{I}{2}\left(1 - \frac{\alpha_\parallel + \alpha_\perp}{2} L - \frac{L}{2}\Delta\alpha \cos 2\beta - \frac{\omega L}{c}\Delta n \sin 2\beta\right) \tag{10.50}$$

with $\Delta\alpha = \alpha_\parallel - \alpha_\perp$ and $\Delta n = n_\parallel - n_\perp$.

The difference of the two transmitted intensities

$$\Delta_1 = I_t(\beta = 0^\circ) - I_t(\beta = 90^\circ) = IL\Delta\alpha/2 \tag{10.51}$$

gives the pure dichroism signal (anisotropic saturated absorption) while the difference

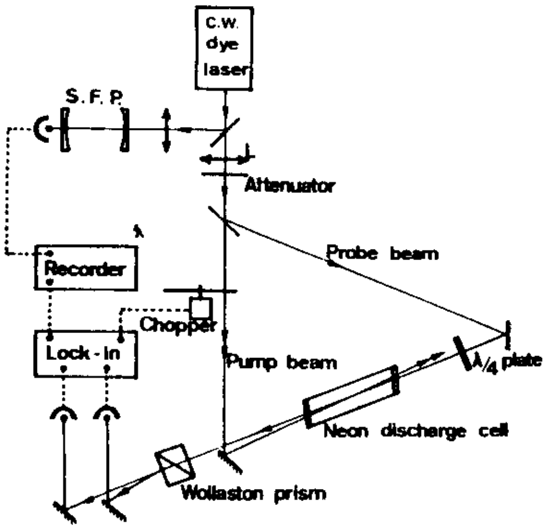

Fig.10.44. Experimental arrangement for observation of Doppler-free laser-induced dichroism and birefringence [10.62]

$$\Delta_2 = I_t(45^0) - I_t(-45^0) = I(\omega L/c)\Delta n \qquad (10.52)$$

yields the pure birefringence signal (saturated dispersion). A birefringent Wollaston prism after the interaction region allows the spatial separation of the two probe beam components with mutual orthogonal polarizations. The two beams are monitored by two identical photodiodes and after a correct balance of the output signals a differential amplifier records directly the desired differences Δ_1 and Δ_2 if the axes of the birefringent prism have suitable orientations.

Figure 10.45 illustrate the advantages of this technique. The upper spectrum represents a "Lamb peak" in the intracavity saturation spectrum of the neon line (1s → 2p) at λ = 588.2 nm (see Sect.10.2). Due to the collisional redistribution of the atomic velocities a broad and rather intense background appears in addition to the narrow peak. This broad structure is not present in the dichroism and birefringent curves (b) and (c). This improves the signal-to-noise ratio and the spectral resolution. Analogous to the technique of "polarization labelling", this method can be extended to optical-optical double-resonance techniques using two different lasers for pump and probe. Signals appear if both lasers are tuned to transitions which share a common level.

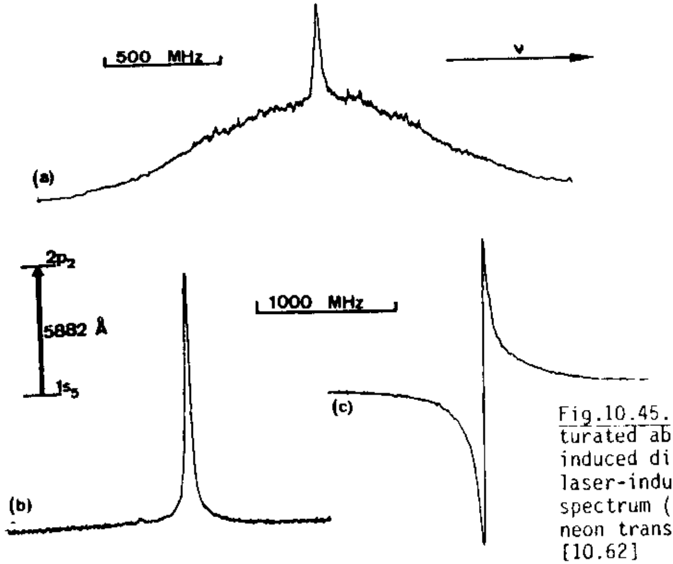

Fig.10.45. Comparison of saturated absorption (a), laser-induced dichroism (b), and laser-induced birefringence spectrum (c) of the $1s_2$-$2p_2$ neon transition at λ = 588.2 nm [10.62]

10.4 Saturated Interference Spectroscopy

The higher sensitivity of polarization spectroscopy compared with conventional saturation spectroscopy results from the detection of *phase differences* rather than amplitude differences. This advantage is also used in a method which monitors the interference between two probe beams where one of the beams suffers saturation-induced phase shifts. This saturated interference spectroscopy was independently developed in different laboratories [10.63,64]. The basic principle can be easily understood from Fig.10.46. We follow here the presentation in [10.63].

The probe beam is split by the plane parallel plate Pl_1 into two beams. One beam passes through that region of the absorbing sample which is saturated by the pump beam; the other passes through an unsaturated region of the same sample cell. The two beams are recombined by a second plane parallel plate Pl_2. The two carefully aligned parallel plates form a Jamin interferometer [4.12] which can be adjusted by a piezoelement in such a way that without the saturating pump beam the two probe waves with intensities I_1 and I_2 interfere destructively.

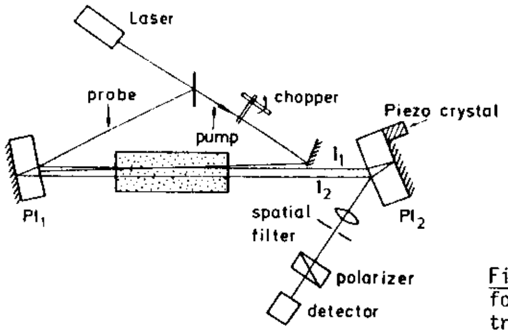

Fig.10.46. Experimental arrangement for saturated interference spectroscopy [10.63]

If the saturation by the pump wave introduces a phase shift ϑ, the resultant intensity at the detector becomes

$$I = I_1 + I_2 - 2\sqrt{I_1 I_2}\cos\vartheta \quad . \tag{10.53}$$

The intensities I_1 and I_2 of the two interfering probe waves can be made equal by placing a polarizer P_1 into one of the beams and a second polarizer P_2 in front of the detector. Due to a slight difference δ in the absorptions of the two beams by the sample molecules, their intensities at the detector are related by

$$I_1 = I_2(1 + \delta) \quad \text{with} \quad \delta \ll 1 \quad .$$

For small phase shifts $\vartheta(\vartheta \ll 1)$ we can approximate (10.53) by

$$I = \left(\frac{1}{4}\delta^2 + \vartheta^2\right)I_2 \quad . \tag{10.54}$$

The amplitude difference δ and the phase shift are both caused by selective saturation of the sample through the monochromatic pump wave which travels in the opposite direction. Analogous to the situation in polarization spectroscopy we therefore obtain Lorentzian and dispersion profiles for the frequency dependence of both quantities

$$\delta(\omega) = \frac{\Delta\delta_0}{1 + x^2} \quad ; \quad \vartheta(\omega) = \frac{1}{2}\Delta\delta_0\frac{x}{1 + x^2} \quad , \tag{10.55}$$

where $x = (\omega - \omega_0)/\gamma$ and γ is the homogeneous linewidth.

Inserting (10.55) into (10.54) yields, for the total intensity I at the minimum of the interference patterns the Lorentzian profile,

$$I = \frac{1}{4} I_2 \frac{(\Delta\delta_0)^2}{1 + x^2} \quad . \tag{10.56}$$

According to (10.55) the phase differences $\vartheta(\omega)$ depends on the laser frequency ω. However, it can be always adjusted to zero while the laser frequency is scanned. This can be accomplished by a sine wave voltage at the piezoelement which causes a modulation

$$\vartheta(\omega) = \vartheta_0(\omega) + a\sin(2\pi f_1 t) \quad .$$

When the detector signal is fed to a lock-in amplifier which is tuned to the modulation frequency f_1, the lock-in output can drive a servo loop to bring the phase difference ϑ_0 back to zero. For $\vartheta(\omega) \equiv 0$ we obtain from (10.54,55)

$$I(\omega) = \frac{1}{4}\delta(\omega)^2 I_2 = \frac{1}{4}\frac{\Delta\delta_0^2}{(1 + x^2)^2} \quad . \tag{10.57}$$

The halfwidth of this signal is reduced from γ to $(\sqrt{2} - 1)^{\frac{1}{2}}\gamma \approx 0.62\gamma$.

Contrary to the situation in polarization spectroscopy, where for slightly uncrossed polarizers the line shape of the polarization signal is a superposition of Lorentzian and dispersion profiles, here a *pure dispersion* line profile can be obtained without distortion by a Lorentzian term. To achieve this, the output of the lock-in amplifier that controls the phase is fed into another lock-in, tuned to a frequency f_2 ($f_2 \ll f_1$) at which the saturating pump beam is chopped. The output of the first lock-in is always proportional to $\vartheta(\omega)$ since it drives the servo loop to bring $\vartheta(\omega)$ back to zero. The second lock-in filters the desired signal caused by the saturating pump beam out of all other background which may cause a phase shift.

The method has been applied so far to the spectroscopy of Na_2 [10.63] and I_2 [10.64]. Figure 10.47a shows saturated absorption signals in I_2 obtained with a dye laser at $\lambda = 600$ nm with 10 mW pump power and 1 mW probe power. Figure 10.47b displays the first derivative of the spectrum in a) and Fig.10.47c, the first derivative of the saturated dispersion signal.

The sensitivity of the saturated interference technique is comparable to that of polarization spectroscopy. While the latter can be applied only to transitions from levels with a rotational quantum number $J \geq 1$, the former works also for $J = 0$. An experimental drawback may be the critical alignment of the Jamin interferometer and its stability during the measurements.